SAND2018-9718R

International Collaboration Activities on Engineered Barrier Systems

Fuel Cycle Research & Development

Prepared for
U.S. Department of Energy

Spent Fuel Waste Science and Technology

Carlos F. Jove-Colon,
Clay Payne,
Andrew Knight
Sandia National Laboratories

August 24, 2018

SAND2018-XXXX

Sandia National Laboratories is a multi-mission laboratory managed and operated by National Technology and Engineering Solutions of Sandia, LLC., a wholly owned subsidiary of Honeywell International, Inc., for the U.S. Department of Energy's National Nuclear Security Administration under contract DE-NA-0003525.

This page is intentionally blank.

AKNOWLEDGEMENTS

The author acknowledges our gratitude to Yifeng Wang (SNL), William Spezialetti (DOE NE-53), Prasad Nair (DOE NE-53), Mark Tynan (DOE NE-53), and Tim Gunther (DOE NE-53) for their helpful discussions and contributions on various topics covered in this report. This work was supported by the DOE-NE SFWST campaign.

This page is intentionally blank.

Table of Contents

List of Tables

Table of Figures

Acronym List

CIEMAT	Centro de Investigaciones Energéticas, Medioambientales y Tecnológicas
CTD	Closure Test Drift
DECOVALEX	DEvelopment of COupled models and their VALidation against EXperiments
DSC	Differential Scanning Calorimetry
DOE	Department of Energy
DOE-NE	DOE Office of Nuclear Energy
DR	Disposal Research
EBS	Engineered Barrier System
EDS	Energy Dispersive Spectroscopy
ED-XRF	Energy Dispersive X-ray Fluorescence
FCT	Fuel Cycle Technologies
FEBEX-DP	Full-scale Engineering Barrier Experiments – Dismantling Project
GREET	Groundwater REcovery Experiment in Tunnel
GTS	Grimsel Test Site
H-C	Hydro-Chemical
JAEA	Japan Atomic Energy Agency
mSEM	Multi (Beam) – Scanning Electron Microscopy
PA	Performance Assessment
QA	Quality Assurance
R&D	Research & Development
SEM	Scanning Electron Microscopy
SFWST	The Spent Fuel Waste Science and Technology
SNL	Sandia National Laboratories
TGA	Thermo-Gravimetric Analysis
THC	Thermal-Hydrological-Chemical
THMC	Thermal-Hydrological-Mechanical-Chemical
TUL	Technical University of Liberec
URL	Underground Research Laboratory
XRD	X-ray Diffraction
XRF	X-ray Fluorescence
µ-XRF	micron X-ray Fluorescence

I. Introduction

International collaborations on nuclear waste disposal is an integral part of the Spent Fuel Waste Science and Technology (SFWST) campaign within the DOE Fuel Cycle and Technology (FCT) program. These engagements with international repository R&D programs provide key opportunities to participate in experiments with international partners on research investigations developing laboratory/field (underground research laboratories (URL) experiments) data of engineered barrier system (EBS) components (e.g., near-field) and characterization of transport phenomena in the host rock (e.g., far-field). The results of these field and laboratory experiments are used in the evaluation of coupled processes and the development of state-of-the-art simulation approaches to evaluate repository performance. Thermal heating from radionuclide decay in the waste canisters will increase temperature in the surrounding EBS driving chemical and transport processes in the near- and far-field domains of the repository. URL heater-tests for extended periods of times (e.g., years) provide key information and data of thermal effects on barrier responses to temperature and water saturation levels.

Description of the various URL experiments for various disposal design concepts according to the host country repository program and relevance to the US program is given elsewhere (Birkholzer et al., 2016; Jové Colón et al., 2016). This part of the report will focus on two international activities within the disposal in argillite work package: FEBEX-DP and DECOVALEX Task C. The FEBEX-DP project focuses on the dismantling of heater #2 (see Fig, 1) conducted during 2015 with the goal of disassembling all the remaining sections of the FEBEX "in situ test" after 18+ year of heating and collection of sensor/probe data (García-Siñeriz et al., 2016; Martinez et al., 2016). Participation in the FEBEX-DP project not only facilitates international partners to access monitoring data but also to samples collected for *post-mortem* characterization of barrier materials obtained during heater dismantling. Birkholzer et al. (2017) describes previous work on bentonite-cement interfaces for FEBEX-DP epoxied overcored samples using micro-X-ray fluorescence (µ-XRF) Multi-SEM (mSEM) scanning probe methods at the micron-scale. The DECOVALEX-2019 Task C involves collaboration with the GREET (Groundwater REcovery Experiment in Tunnel) at the Mizunami URL, Japan, which targets the development of monitoring methodologies of groundwater in granitic rock with applications to THMC simulations (Iwatsuki et al., 2005; Iwatsuki et al., 2015). The focus of GREET is to conduct a facility-scale geochemical characterization study of short- and long-term effects of tunnel excavation activities, impacts on groundwater flow and transport, and influences on groundwater chemistry (Iwatsuki et al., 2015). The data obtained from these URL activities is then used in the development and evaluation of THC models to support post-closure safety and performance assessments of the repository environment.

The main goals of this report section in each of the international activities are:

- FEBEX-DP:
    - Analysis of a FEBEX-DP bentonite samples from Section 49 using X-ray Fluorescence (XRF), X-ray diffraction (XRD), and thermogravimetric analysis (TGA/DSC) analytical techniques. These analytical approaches are conducted on samples collected as a function of distance from the gallery center or heater surface.
- DECOVALEX Task C:
    - 3D Reactive transport modeling of the closure test drift (CTD) focusing on shotcrete – ground water interactions of the cement liner in the water-filled tunnel. This simulation effort is part of an inter-comparison exercise between different modeling teams (SNL, JAEA, TUL) in this task.

II. FEBEX-DP: X-ray Fluorescence (XRF) and X-ray diffraction (XRD) Studies of Bentonite from Section 49

The FEBEX-DP project currently entails the dismantling of heater #2 (see Fig. 1) performed during 2015 with the goal of carefully retrieving barrier material samples from the remaining sections of the FEBEX "in situ test" after 18+ year of heating which also includes sensor/probe data (García-Siñeriz et al., 2016; Martinez et al., 2016). This disassembling activity involves sampling of barrier bentonite, steel liner, sensors, embedded metallic components (e.g., metal coupons), and near-field sections with tracer components. The FEBEX bentonite is composed of ~93% smectite with 2% quartz, 3% plagioclase, and 2% cristobalite plus minor accessory phases such as calcite and K-feldspar (Huertas et al., 2000; Missana and García-Gutiérrez, 2007). The focus of this study is to conduct XRF, XRD, and TGA/DSC studies on FEBEX-DP samples from section 49 corresponding to spatial domains near and far from the surface of heater #2 (see Fig. 2 for sample locations). Fig. 3 shows the radial locations of samples collected in Section 49 considered in this study.

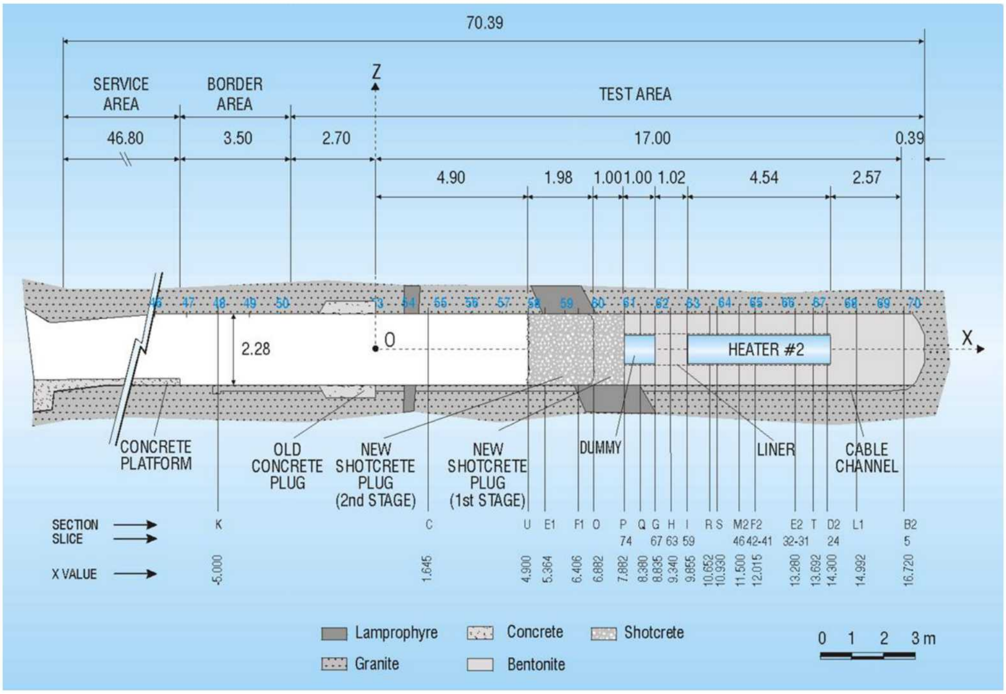

Figure 1. Schematic layout of the FEBEX "in-situ" field test after the first partial dismantling showing the configuration of heater #2 at the GTS URL (García-Siñeriz et al., 2016).

Previous studies (Birkholzer al., 2017) on Section 49 were centered on SEM/EDS characterization of samples closest to the corroded carbon steel mesh surrounding the heater. These studies revealed sparse Al-Si grains high in Fe immersed correlated with some enrichment of K in certain cases. These grains are immersed in the clay matrix and can be singled out due to their different texture. The extent of the corroded region into the bentonite is rather limited which might explain the relatively low level of Fe alteration into the bentonite, particularly in the hotter zones of the heater. The main objective of this characterization study is to (1) identify bulk compositional and structural (also mineralogical) variations (XRF and XRD, respectively) of bulk bentonite samples near and far from the heater surface, (2) similarly, conduct TGA/DSC thermal analyses of these samples, and (3) compare results with those obtained by other teams for other sampled sections of the bentonite barrier as part of the FEBEX-DP project.

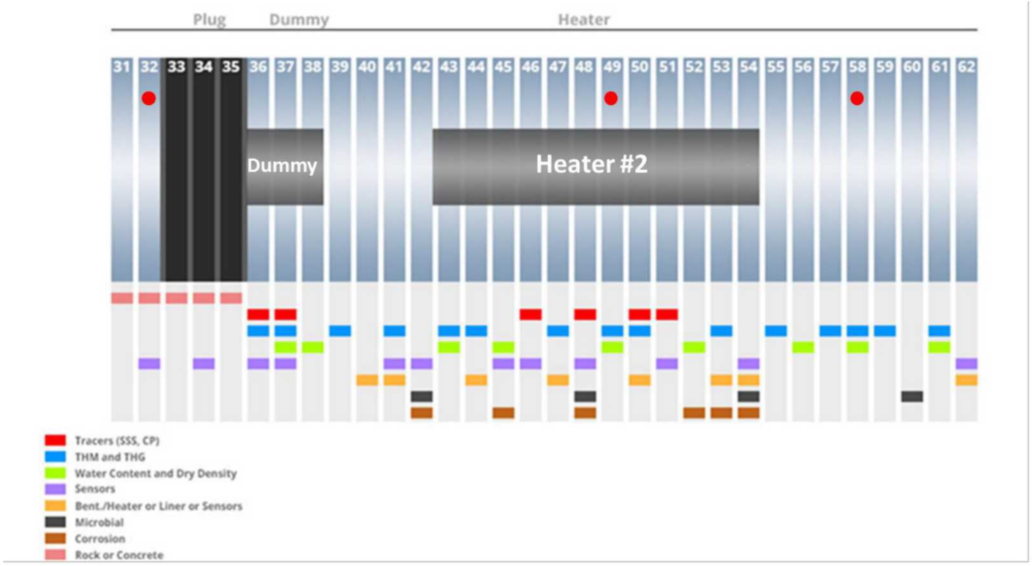

Figure 2. Schematic configuration of sampling zones (indicated by vertical light blue bars) for the FEBEX-DP project. Filled red circles indicate zones for samples obtained by Sandia National Laboratories (SNL). Source: FEBEX-DP website (members area): http://www.grimsel.com/gts-phase-vi/febex-dp/febex-dp-introduction.

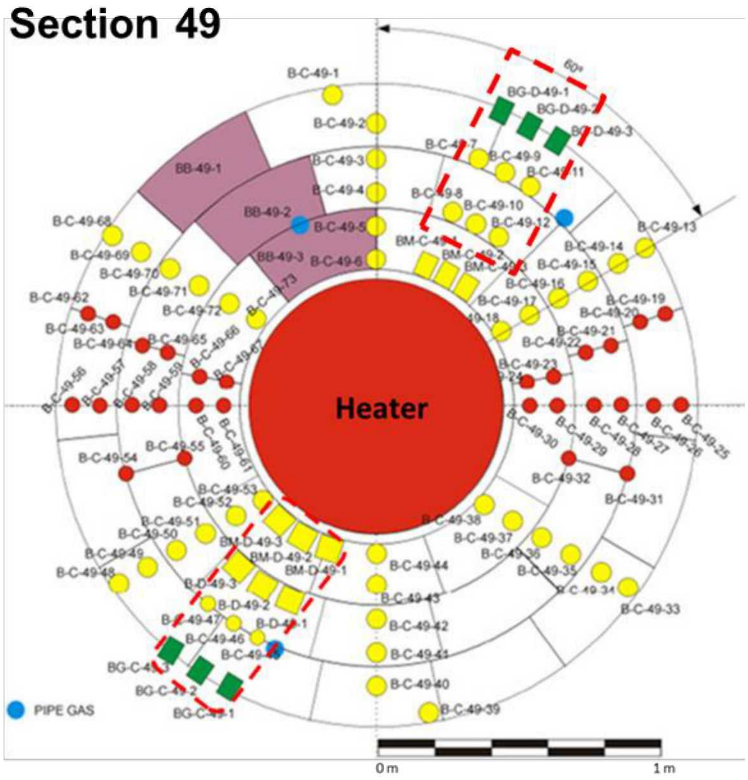

Figure 3. Schematic diagram of sampling locations for the FEBEX-DP dismantling of section 49. See Fig. 2 for section location relative to the heater zone. The red-dashed line delineates the locations of samples analyzed in this study (source: FEBEX-DP website (members area): http://www.grimsel.com/gts-phase-vi/febex-dp/febex-dp-introduction.). Note: samples BG-C-49 (1, 2, 3) were not analyzed with XRF in the current study. Their analysis is planned as part of future work on these samples.

III. Methodology: XRF, XRD, and Thermal Analyses (TGA/DSC)

XRF and TGA Study

Thermal loads during the post-closure period can drive barrier alteration due to enhanced interactions with fluids, induced phase transformation, and changes in bentonite under unsaturated conditions. Jove Colon (2016) describes the 2D-3D characterization of microcracks in FEBEX-DP shotcrete-bentonite overcore outlining the importance of desiccation/shrinkage processes in bentonite and the nature of pores/voids in shotcrete. Mineral dissolution and precipitation along with transport which has been a topic of investigation particularly in the assessment of engineered barrier alteration in reactive-transport models (Marty et al., 2015; Wilson et al., 2015; Xie et al., 2015). An example is Fe-bentonite interactions which leading to mineral phase changes that could impact swelling capacity in bentonite through alteration to a non-swelling Fe-bearing phase. Also, cation exchange in the bentonite clay could also be impacted through temperature-induced drying and wetting causing variations in the cation exchange capacity (CEC) (Muurinen, 2011). Cation exchange experiments reported by Villar et al. (2017) show that FEBEX-DP bentonite samples collected from sections closest to the heater exhibit higher concentrations of exchangeable Mg and Ca and low concentrations of exchangeable Na. Moreover, aqueous extracts for bentonite samples collected in sections close to the heater exhibited higher aqueous concentrations of Mg, Ca, Na, and Cl relative to those sampled farther away from the heater. It should be noted that the aqueous extract process is influenced by ion exchange and solid phase dissolution (Villar et al., 2017). These relatively strong changes in the observed aqueous concentration behavior from these tests indicate that bentonites close to the heater are affected by thermal effects causing changes in the bentonite clay mineral and therefore their interaction with fluids. It would then be expected that such effects on bentonite sorption behavior could be manifested in the bulk clay composition.

The FEBEX-DP effort has documented bulk XRF bentonite compositional analyses with distance from the heater for various sampled sections of the EBS (Villar et al., 2017). Such compositional profiles as a function of sample radial location could provide key information of clay chemical variability, plausibly in response to thermal perturbations. Samples collected in section 49 experienced the hottest part of the heater given its location close to the center of the (cylindrical) heater longitudinal axis. XRF data of these will be analyzed and compared to data reported in Villar et al. (2017) for other samples collected along other sections of the heater.

Sample Preparation

Samples were prepared and analyzed as <150 μm, <75 μm, and <2μm fractions. The <150 μm and >75 μm fractions were prepared by grinding and sieving through a final sieve of 100 mesh and 200 mesh, respectively. The <2μm fraction samples were prepared by a sedimentation method as described by McKay (1992). The <75 μm fraction was transferred to a 1 L graduated cylinder. The cylinder was filled with Mili-Q H_2O (Barnstead NANOpure Diamond, resistivity of 18.2 MΩ*cm, 0.2 μm filtered and UV irradiated) up to the 30 cm mark. The top was capped and the cylinder was inverted several times to ensure adequate mixing. The contents were allowed to settle for 24 hours. After 24 hours, the remaining suspended clay was decanted into centrifuge bottles (250 mL) and centrifuged at 3000 rpm for 20 minutes. The collected liquid was decanted again and the solids were combined and place in the oven to dry at 60°C for 48+ hours.

XRF and TGA/DSC Analyses

Samples were loaded into an XRF sample cup (31 mm by 23.1 mm, double open ended cup, Chemplex Industries, Inc., Palm City, FL) equipped with microporous film (25 μm thick, Chemplex Industries, Inc.) and analyzed with an Quant'X ARL Energy Dispersive (ED)-XRF (ThermoFisher Scientific, Waltham, MA). A method file was prepared in the Wintrace 7.2 software. In the method, the peak profiles were loaded and the analysis conditions were selected. These conditions consisted of low Z_a (4 kV, no filter), low Z_b (8 kV, cellulose filter), low Z_c (12 kV, aluminum filter), mid Z_a (16 kV, thin palladium filter), and high Z_b (50 kV, thick copper filter). Each condition was run under vacuum for 500 second live time, with an average of 50% detector dead time. A calibration was performed using fundamental parameters method and XML composition calculation. The standards used for the calibration were SARM 1, SARM 3, SARM 4, SARM 5, SARM 6 and CAMET SY-2, CANMET SY-3, and CANMET MRG-1, the composition of the major elements in each standard are shown in Table 1. Following the calibration, the bentonite samples were analyzed in triplicate and the percent composition was calculated as an average of the triplicate analyses. The water content was estimated from data obtained from thermogravimetric analysis (TGA), and the carbon content was estimated by the mass difference. The latter is just an estimate and more accurate methods are required to determine carbon in this samples.

Table 1. Composition of standards used for the ED-XRF calibration*.

	SARM-1	SARM-3	SARM-4	SARM-5	SARM-6	CANMET Sy-2	CANMET S-3	CANMET MRG-1
SiO_2	75.70 %	52.40 %	52.64 %	51.10 %	38.96 %	60.07 %	59.71 %	39.22 %
Al_2O_3	12.08 %	13.64 %	16.50 %	4.18 %	0.3 %	12.15 %	11.70%	8.51%
Total Fe	2.00 %	9.9 %	8.97 %	12.70 %	17.00 %	6.32 %	6.47 %	17.93 %
CaO	0.76 %	3.22 %	11.50 %	2.66 %	0.28 %	2.66%	2.63 %	13.49 %
Na_2O	3.36 %	8.37 %	2.46 %	0.37 %	0.04 %	8.03 %	8.30 %	14.68 %
K_2O	4.99 %	5.51 %	0.25 %	0.09 %	0.01 %	4.37 %	4.17 %	0.72 %
F	0.42 %	0.44 %	-	-	-	-	0.02 %	0.01 %
H_2O^+	0.49 %	2.31 %	0.33 %	0.26 %	0.30%	4.52 %	4.20 %	0.18 %
MgO	0.06 %	0.28 %	7.50 %	25.33 %	43.51 %	3.61 %	3.61 %	8.61 %
TiO_2	540 ppm	-	-	0.20 %	-	0.49 %	0.36 %	1.04 %
S	-	650 ppm	-	-	-	-	-	-
P_2O_5	-	-	-	90 ppm	40 ppm	0.03 %	0.04%	-

* Units in weight percent unless noted.

Thermal gravimetric analysis (TGA) and differential scanning calorimetry (DSC) analysis were conducted on all <150 μm and <2 μm bentonite fractions. The <75 μum fraction was not analyzed as it was assumed that very little changes would occur following additional sieving from 150 μm to 75 μm particle sizes. The analyses were performed using a Thermal Analyst SDT Q6000 instrument. The furnace chamber was purged with a 100 mL/min flow of ultra-pure Argon (Ar). An alumina crucible was tarred and filled with roughly 20-40 mg of bentonite. After loading the furnace with the sample, the analysis procedure consisted of (1) an isothermal step for 20 minutes at room temperature followed by (2) a ramped temperature stepping of 10°C/min from 20 to 1100 °C. The water content was estimated by the total weight loss.

IV. Results and Discussion: FEBEX-DP Section 49

XRF and TGA/DSC Analyses

Figures 4 to 7 summarize all the collected XRF elemental data along with data reported by Villar et al. (2017). The analyzed oxides are SiO_2, Al_2O_3, MgO, CaO, Na_2O, K_2O, TiO_2, and Fe_2O_3. As shown in Fig. 4, SiO_2 content falls within the ranges of data reported by Villar et al. (2017) but tending towards lower concentration bounds below reference values for FEBEX bentonite. Similarly, Al_2O_3 content mainly falls within the range of the lower bounding data for FEBEX reference values with no apparent correlation with distance from the gallery center.

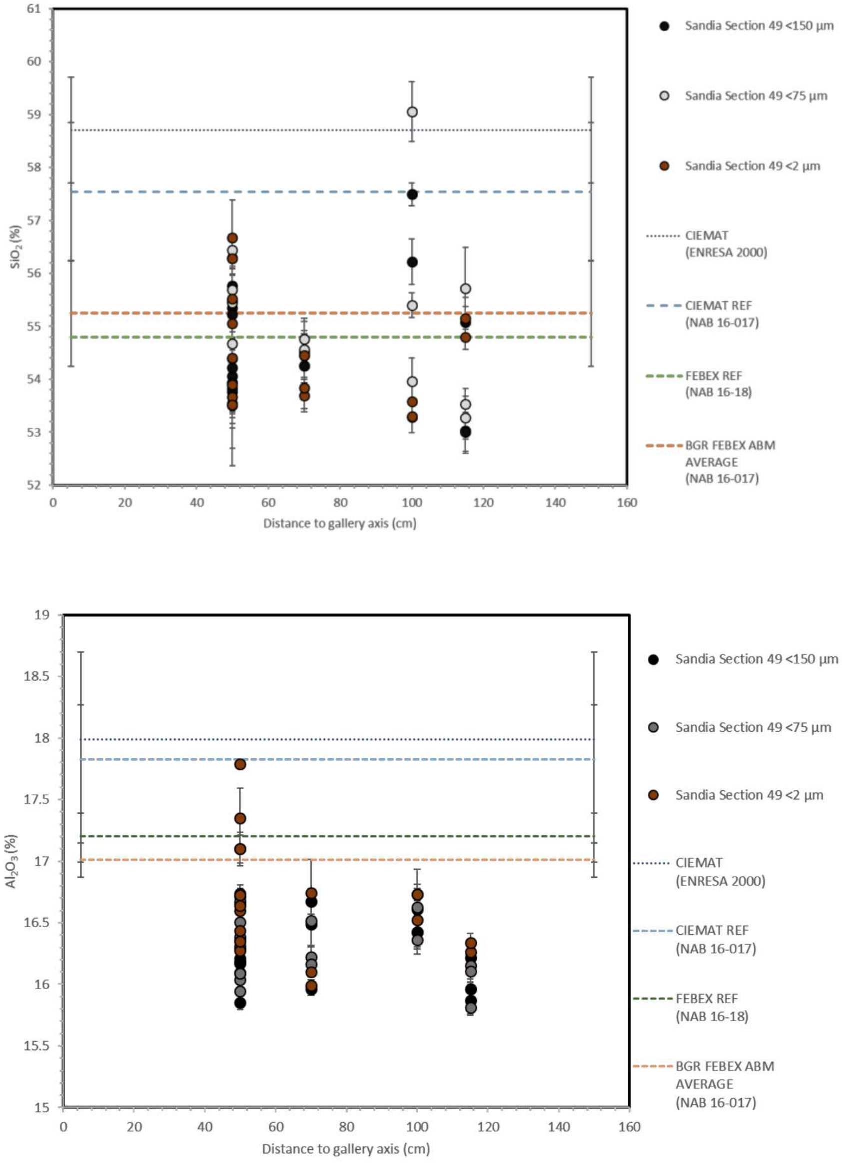

Figure 4. Bulk bentonite XRF analyses of SiO_2 (upper) and Al_2O_3 (lower) contents for Section 49 samples as a function of distance from the gallery axis. Filled symbols denote analyses conducted in this study for size fractions of <150, <75, and <2 microns. Horizontal dashed-lines delineate the range of FEBEX bentonite compositions including reference values by different groups (Villar et al. 2017).

Fig. 5 shows a comparison of MgO and CaO contents between Section 49 samples in this study and analyses from other sections reported by Villar et al. (2017). Notice that MgO content increases with decreasing distance from the heater or towards the heater surface (~50 cm from the gallery center). The same trend is observed for other samples surrounding the heater (S45, S48, S50, S53), particularly for sample S48 which like S49 experienced the hottest location of the heater (Villar et al., 2017). Similar observations were made by Villar et al. (2017) for exchangeable Mg where its largest concentration was observed in samples close to the heater. Also, most of our MgO content data lies above the FEBEX reference values. The Mg enrichment in bentonite close to the heater could potentially affect the swelling behavior and sorption properties of the clay. CaO content data doesn't show a clear correlation with distance from the gallery center. However, Villar et al. (2017) noticed a slight overall enrichment of CaO content towards the gallery walls. Overall, measured CaO contents are spread above and below the bounds for the FEBEX reference values.

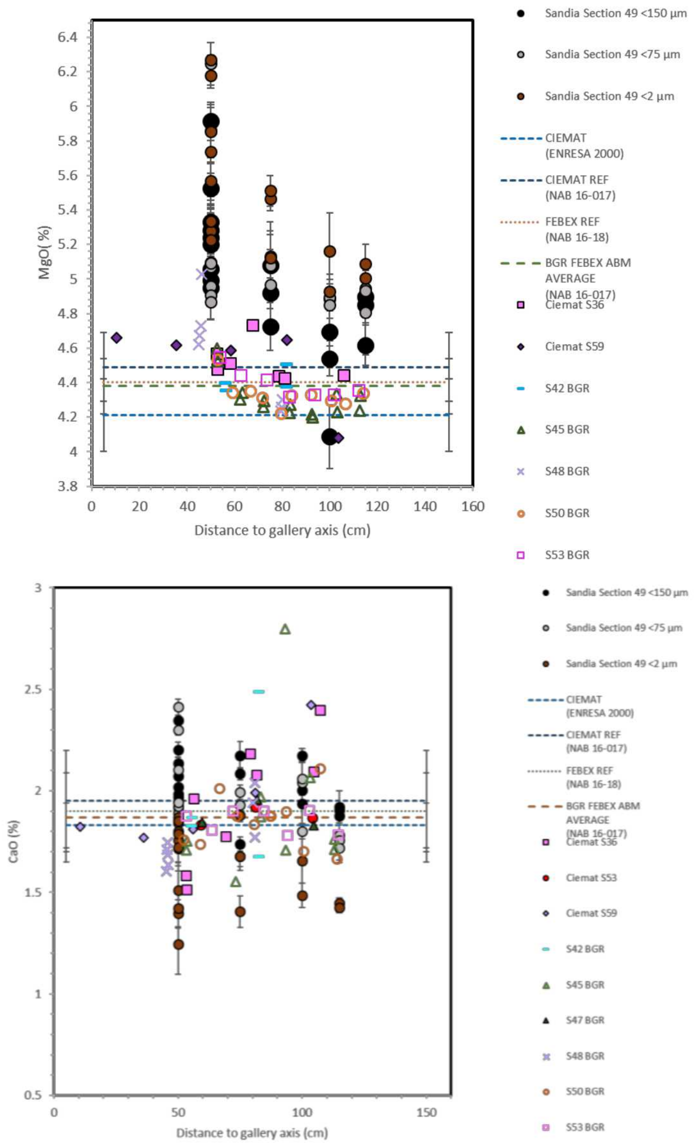

Figure 5. Bulk bentonite XRF analyses of MgO (upper) and CaO (lower) contents for Section 49 samples as a function of distance from the gallery axis. Filled circles denote analyses conducted in this study for size fractions of <150, <75, and <2 microns. Horizontal dashed-lines delineate the range of FEBEX bentonite compositions including reference values by different groups (Villar et al. 2017).

Fig. 6 shows a comparison of Na_2O and K_2O contents between Section 49 samples in this study and analyses from other sections reported by Villar et al. (2017). As in CaO, our data for Na_2O content doesn't show a clear correlation with distance from the gallery center. Limitations in Na detection in the XRF method of our study produces data with large uncertainties and therefore resolving apparent data trends with distance from the gallery center is difficult. Na_2O content reported by Villar et al. (2017) decreases towards the surface of the heater as shown in Fig. 6. Such trend is opposite to that of MgO probably suggesting ion exchange enhanced with increasing temperatures. Overall, K_2O content tends to decrease towards the heater with values within and below the ranges of the FEBEX reference data bounds. The <2 microns fraction data show this decreasing K_2O content trend towards the heater and bounds data below the FEBEX reference values.

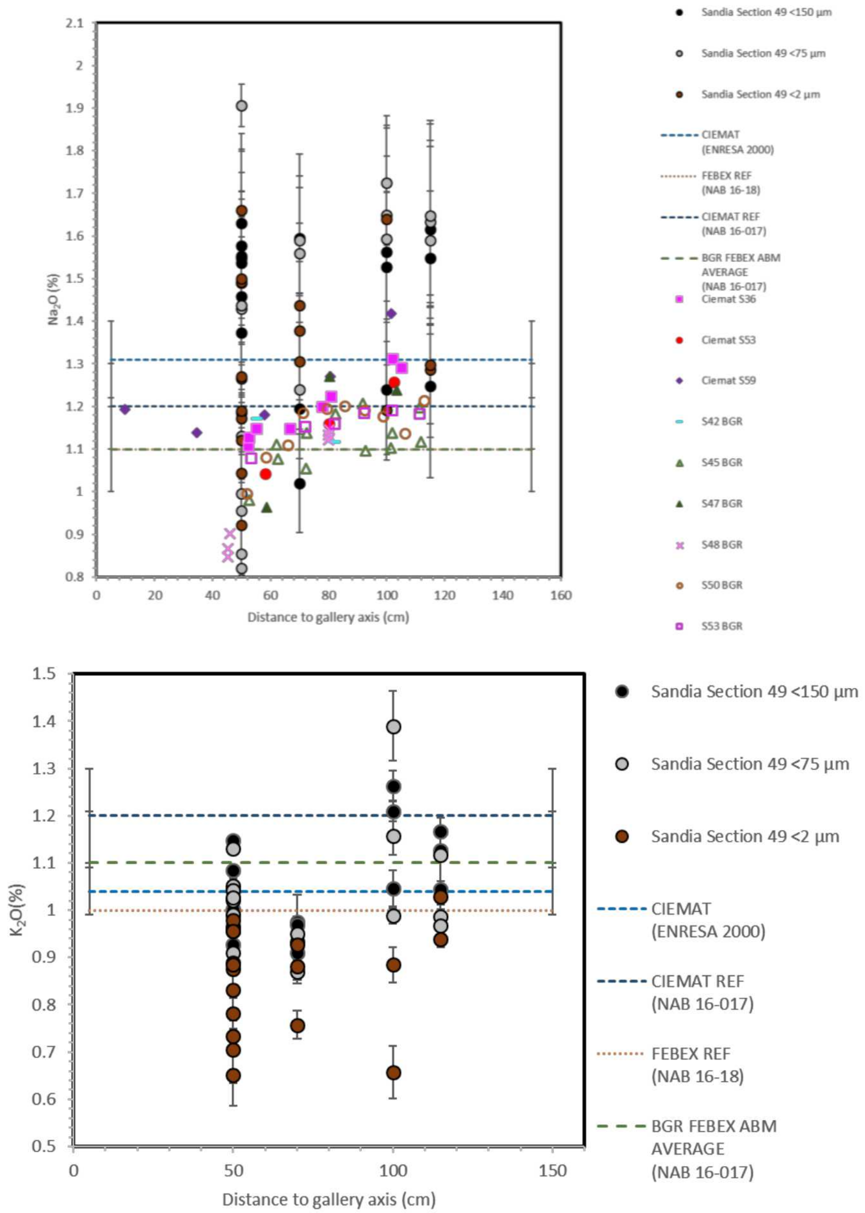

Figure 6. Bulk bentonite XRF analyses of Na_2O (upper) and K_2O (lower) contents for Section 49 samples as a function of distance from the gallery axis. Filled circles denote analyses conducted in this study for size fractions of <150, <75, and <2 microns. Horizontal dashed-lines delineate the range of FEBEX bentonite compositions including reference values by different groups (Villar et al. 2017).

The reason for the lower values in this finer fraction is probably due to the presence of K-bearing minerals (e.g., feldspar) separated during the settling procedure. Similarly, Fig. 7 shows the distribution of TiO_2 and Fe_2O_3 content generally decreasing towards the heater, particularly for the finer fraction. For clarity, Figs. A-1 through A-8 in Appendix A show the same data as in Figs. 1 through 7 but plotted separately as a function of distance from gallery center for each size fraction.

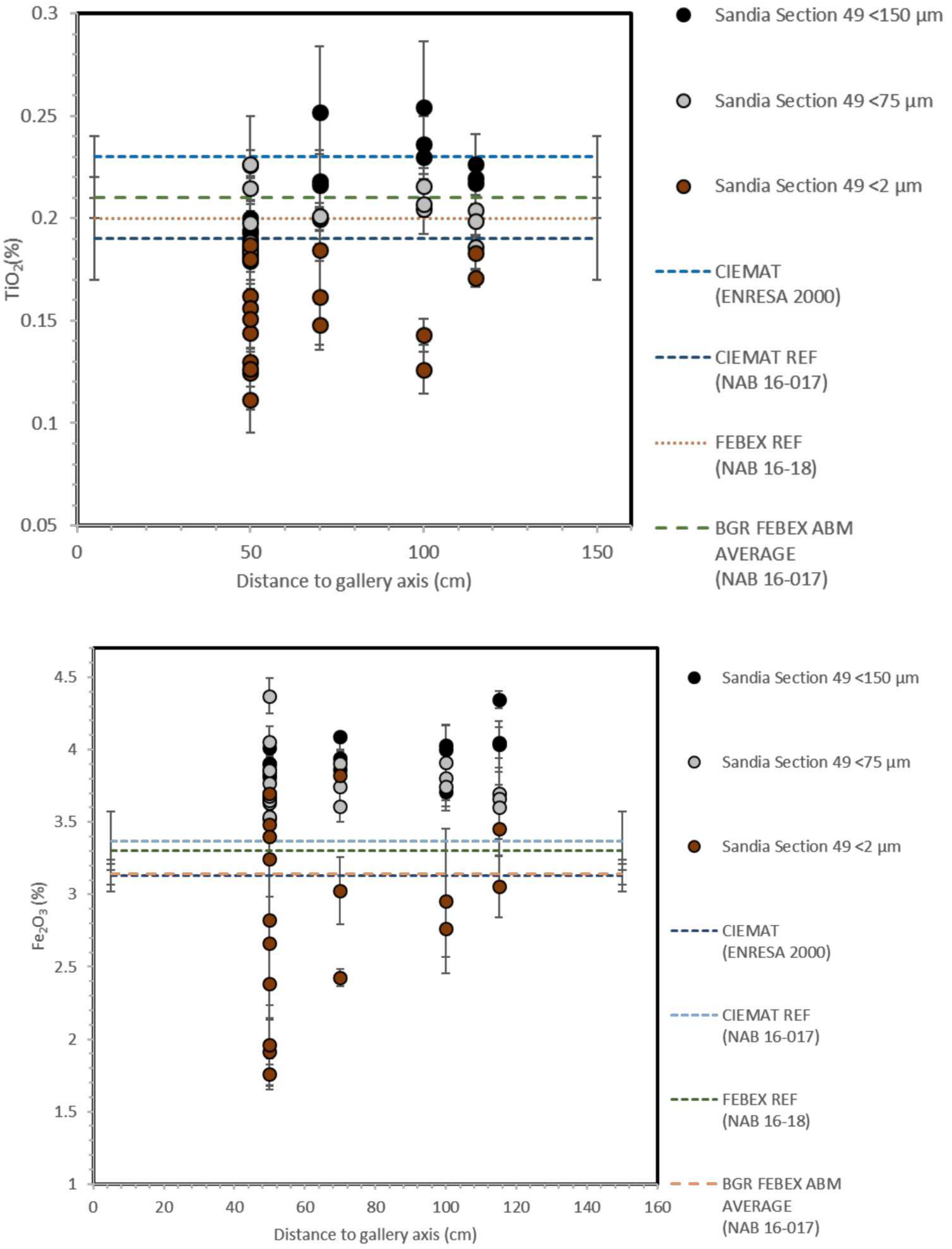

Figure 7. Bulk bentonite XRF analyses of Ti_2O (upper panel) and Fe_2O_3 (lower panel) content for Section 49 samples as a function of distance from the gallery axis. Filled circles denote analyses conducted in this study for size fractions of <150, <75, and <2 microns. Horizontal dashed-lines delineate the range of FEBEX bentonite compositions including reference values by different groups (Villar et al. 2017).

TGA and DSC data are summarized in Fig. 8 for all the considered samples as a function of distance from the gallery axis. Fig. 9 shows the retrieved water content as a function of distance from gallery axis. The outlier sample with lowest water content (B-C-49-1; uppermost curve in the TGA mass loss and smallest water content value in Figs. 8 and 9, respectively) was located next to a gas pipe within the bentonite barrier. This may explain the much lower water content relative to the other samples. DSC data shows a strong endothermic peak around 100-110 °C but also reaching temperatures of 120-125 °C in some samples. This peak corresponds to dehydration of adsorbed water at clay hydration sites (Tajeddine et al., 2015; Vieillard et al., 2016). The TGA analyses reported in Villar et al. (2017) on FEBEX bentonite samples from Section 47 appears to show slightly higher temperature values (~136°C) for this first endothermic peak. The second endothermic peak around 650°C is consistent with the range of dehydroxylation temperatures observed for smectite clays (Tajeddine et al., 2015; Vieillard et al., 2016; Villar et al. 2017). Overall, the water content data retrieved from TGA (Fig. 9) show a spread of values with no clear dependency with distance from gallery axis or the heater surface located at ~50 cm from the gallery axis. Water content data reported by Villar et al. (2017) clearly shows an increasing trend with distance from the gallery axis. However, such a trend was not observed from our TGA data plausibly due to differences in the adopted methodologies to quantify water content. In the TGA method the bentonite sample is exposed to 110°C for 10 minutes. Water content data reported in Villar et al. (2017) was obtained through heating the sample at 105-110 °C from 2 to 7 days.

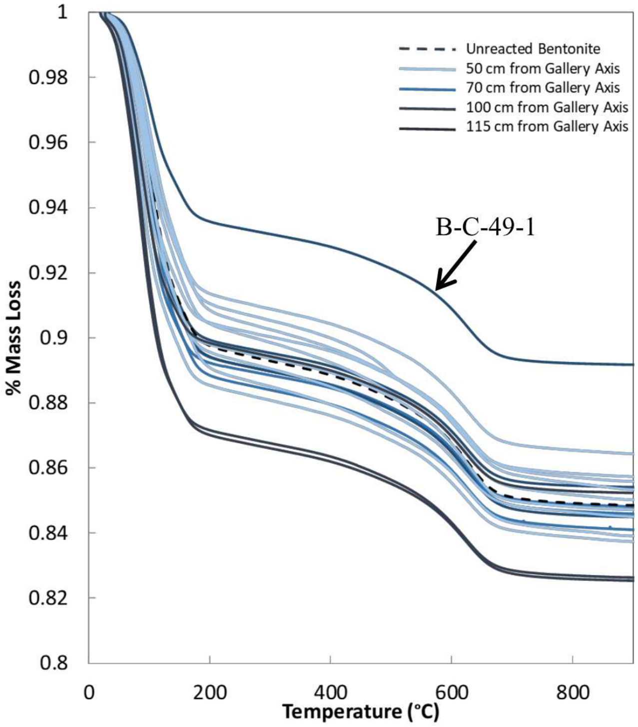

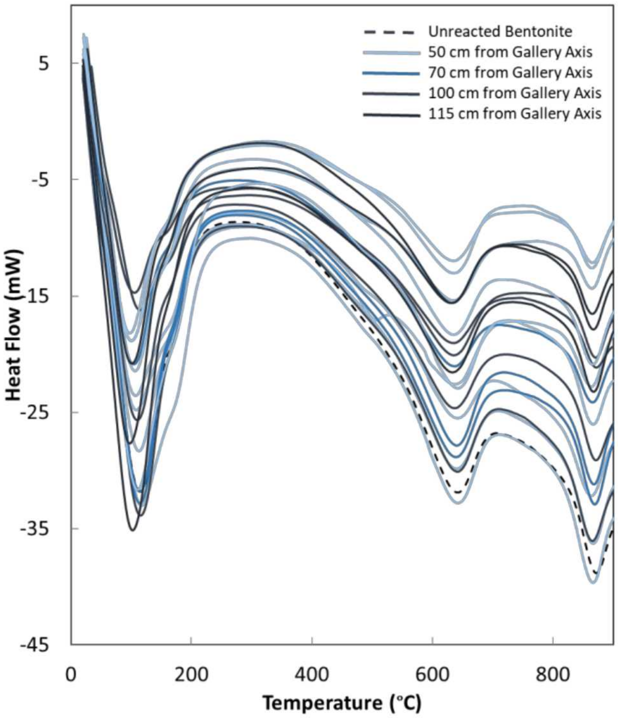

Figure 8. Thermogravimetric analysis (TGA) and differential scanning calorimetry (DSC) measurements of bentonite samples for Section 49 as a function of distance from gallery axis. Dashed-line represents the unreacted FEBEX bentonite. Outlier (uppermost) curve in TGA upper figure represents sample B-C-49-1 located next to a gas pipe within the bentonite barrier (see schematic Fig. 3 for location).

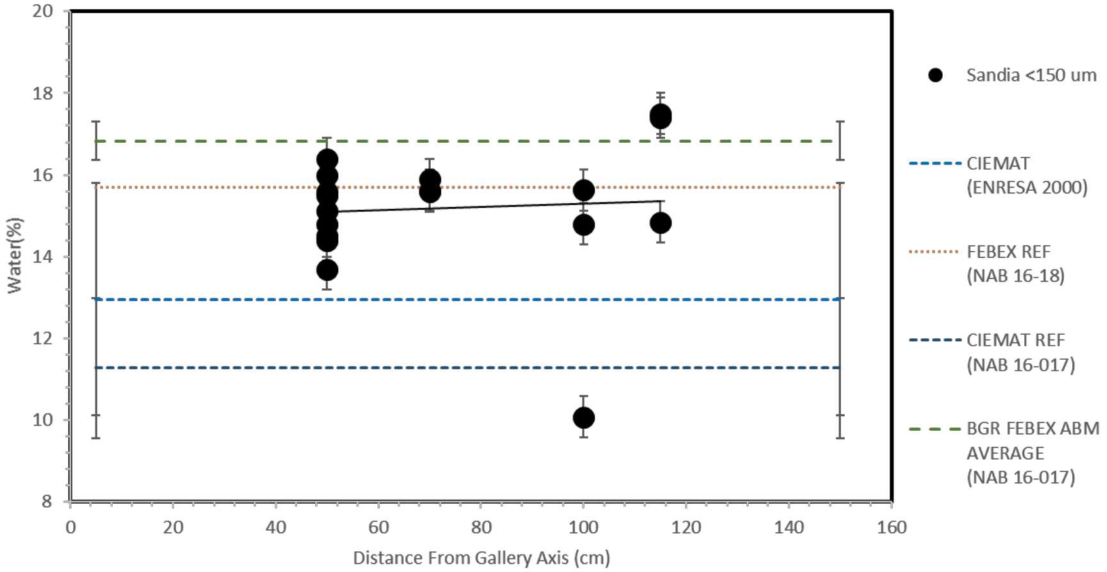

Figure 9. Water content measurements of bentonite samples for Section 49 as a function of distance from gallery axis. Solid line represents the overall trend of the data (see text). Horizontal dashed-lines delineate water content measurements of FEBEX bentonite samples from other studies shown here for comparison. Outlier (lowermost) value represents sample B-C-49-1 located next to a gas pipe within the bentonite barrier (see schematic Fig. 3 for location).

Not considering the outlier, Fig. 9 shows a rather weak tendency towards higher water content with distance from the heater surface. In general, the TGA and DSC curves have a qualitative similar form when compared to the thermal studies by Tajeddine et al. (2015) and Vieillard et al. (2016) on MX-80 montmorillonite, and by Villar et al. (2017) on FEBEX bentonite from other FEBEX-DP sampled sections. Work is planned to conduct an analysis and comparisons between the FEBEX bentonite data sets and the Tajeddine et al. (2015) and Vieillard et al. (2016) studies on MX-80 montmorillonite to evaluate differences in thermal properties between the two bentonite clay compositions.

XRD Methodology

X-ray diffraction (XRD) analyses were conducted on the suite of FEBEX-DP bentonite clay samples analyzed by XRF and TGA/DSC. The focus was to characterize mineral types present in the bentonite matrix and quantify d-spacings (basal d_{001}) of the smectite component. A full matrix of dried and glycol saturated samples varying in distance from the gallery axis were examined.

The powder diffraction data was collected using a Bruker D2 Phaser benchtop diffractometer with a CuKα (1.54 Å) X-ray wavelength. The analysis was conducted in a 2-theta range of 3 -70° with 0.2 s time per step with a total of 2256 steps. This resulted in XRD runs that were ~8.5 minutes in duration. Silicon wafers were chosen as the sample holders for the oriented clay mounts as it provides very low background interference and were optimal for making oriented clay slurry mounts. A desiccator was adapted into a glycolation chamber for the purposes of the project by filling the desiccator with ethylene glycol, then heating the entire desiccator. The heat caused the ethylene glycol to vaporize and create a glycol vapor saturated environment within the desiccator.

Sample preparation consisted first of crushing the clay using a mortar and pestle into small particle sizes to achieve a “powder like” consistency. XRD analysis of dried clay sample consisted of adding ~0.1 g of clay to a 25 mL scintillation vial. 1 mL of a 70-30% water-ethanol mixture was added to the scintillation vial to have a mass/liquid ratio of 0.1. The ethanol was added to the samples to decrease the cracking behavior of the oriented clay samples upon drying. The suspended clay was hand shaken vigorously until clay was sufficiently suspended. Then using a 1000 μL micropipette the slurry was pipetted in a circular motion onto the zero-background silicon wafer. The wafer was then placed in the convection oven between 60-70°C and allowed to dry. After the sample had completely dried, the wafer was placed in the Bruker sample holder to perform the XRD analysis. After completion of XRD analysis of the dried samples, this bentonite material was then placed into a desiccator over a pool of ethylene glycol. The desiccator was then placed in the oven heated at 60°C and left for 24 hours to ensure glycol saturation of the bentonite samples. The following day the sample was removed from the desiccator and the XRD analysis was conducted immediately to ensure the bentonite remained glycol saturated.

XRD Data

Figures 10 through 14 show the representative XRD spectra collected for glycolated samples from Section 49. The spectra are presented as stacked plots with X-ray intensity (Y-axis; arbitrary units) vs. 2θ. XRD spectra for air-dried samples along with its corresponding glycolated profile are given in Figs. A-9 to A-13 in Appendix A. Quantification of bentonite mineralogical composition through XRD was not part of the current study but it is planned for future work. This compositional information can be found in Villar et al. (2017) where a divalent smectite is the main component (~92%) of the FEBEX bentonite. XRD peaks for quartz and feldspar were resolved mainly in the air-dried bentonite samples having similar 2θ ranges as reported in Villar et al. (2017). Calcite was not observed in our samples. Also, no definite evidence of occurrence of illite was found in these samples. XRD peaks for accessory minerals in the bentonite like quartz and feldspar were not observed in some samples, maybe indicative of the variability in their mineralogical content even within the same block or because of limited detection with the XRD method.

In general, comparisons between glycolated bentonite spectra from this study and those from Villar et al. (2017) on FEBEX-DP bentonite samples from other sections show close similarities in the peaks for $d_{00\ell}$ (d_{001}, d_{002}, d_{003}, d_{004}, d_{005}) reflections. The only exception is the d_{006} peak which was not observed in our samples but it was present in the spectra reported for samples BB-53-4 by Villar et al. (2017). The range of $d_{00\ell}$ values are consistent with those reported by Villar et al. (2017). The strong basal (d_{001}) reflections around 13-14 Å is characteristic of Mg-bearing montmorillonites whereas its value of around 16.4 Å for the glycolated samples suggest a state of nearly full interlayer expansion (Teich-McGoldrick et al., 2015). Fig. 15 summarizes the distribution of d_{001} values with distance from the heater for air-dried and glycolated samples. As shown in this figure, there is no clear trend or apparent correlation between d_{001} values and sample radial location with respect to distance from the heater. Values for d_{001} basal reflections are affected by the smectite hydration state and the interlayer cation. However, d_{110} reflections are representative of the smectite structure and are unaffected by interlayer hydration (Grim, 1968). These peaks were resolved in our air-dried samples and their distribution with distance from the heater is shown in Fig. 16. Like the d_{001} distribution in Fig. 15, there is no clear trend with distance from the heater except for the apparent reduced variability in these values for samples closest to the heater.

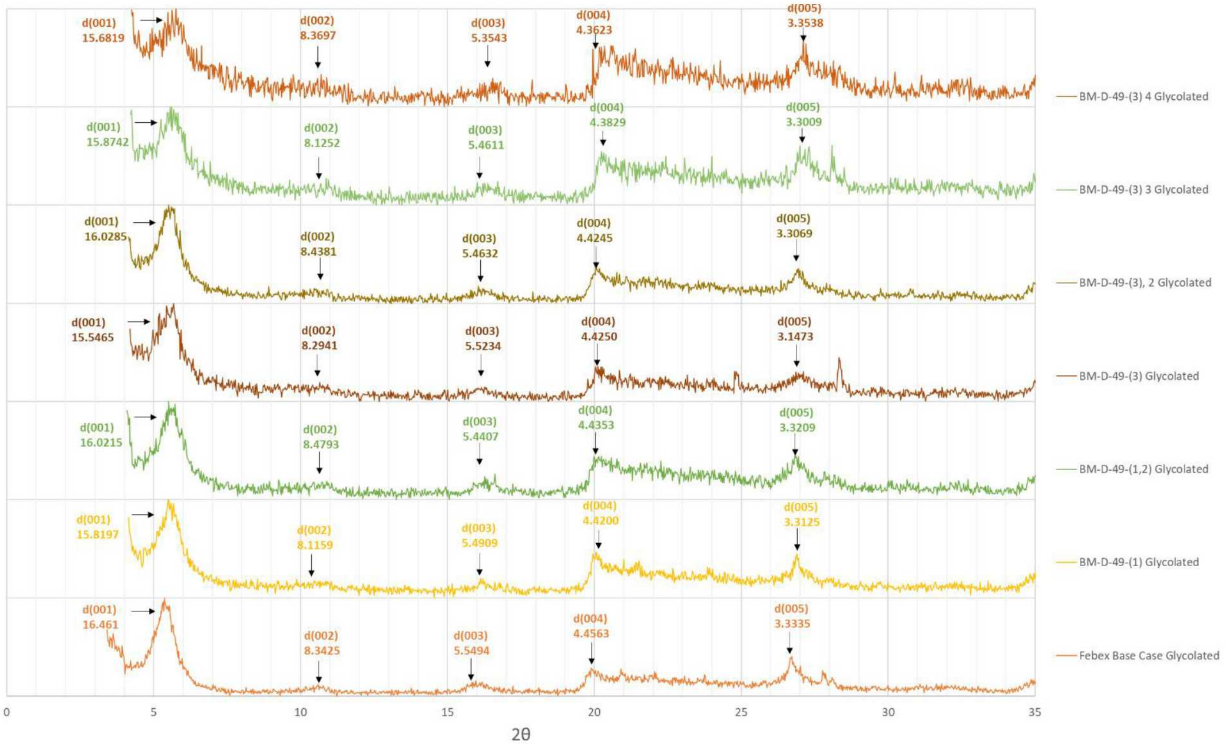

Figure 10. XRD spectra for various positions of BM-D-49 samples in the same blocks along with d-spacings (see schematic Fig. 3 for sample locations). XRD spectrum of FEBEX base case or reference material is shown at the bottom for comparison. These samples are closest to the heater.

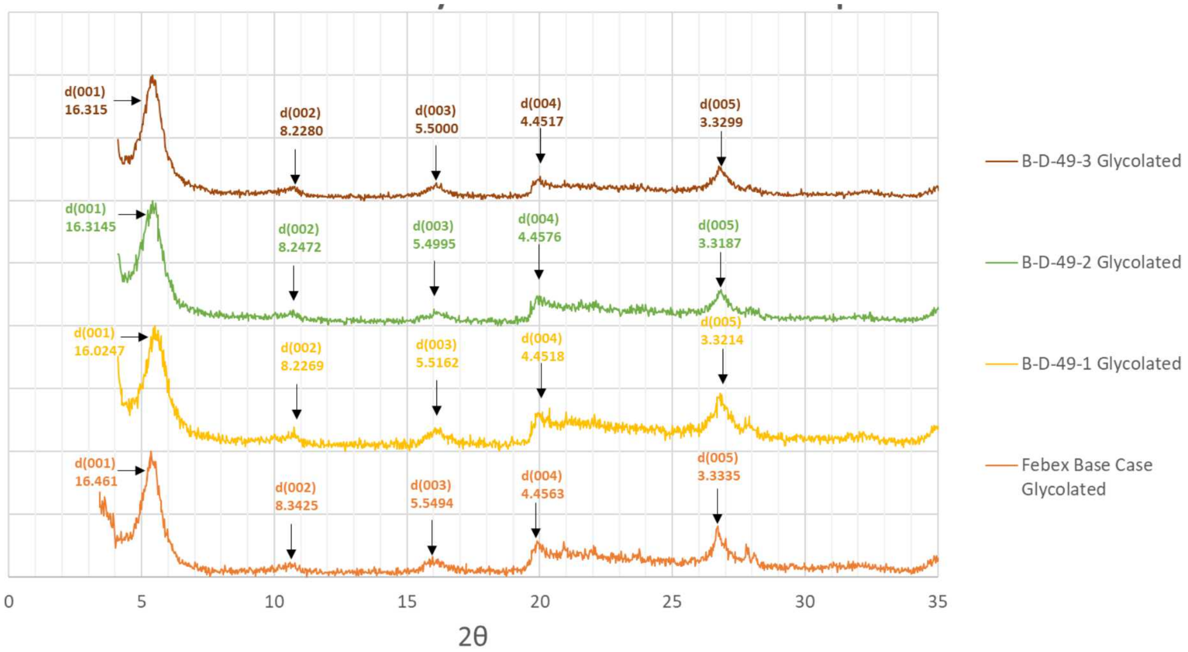

Figure 11. XRD spectra for various locations of B-D-49 block samples along with d-spacings (see schematic Fig. 3 for sample locations). XRD spectrum of FEBEX base case or reference material is shown at the bottom for comparison.

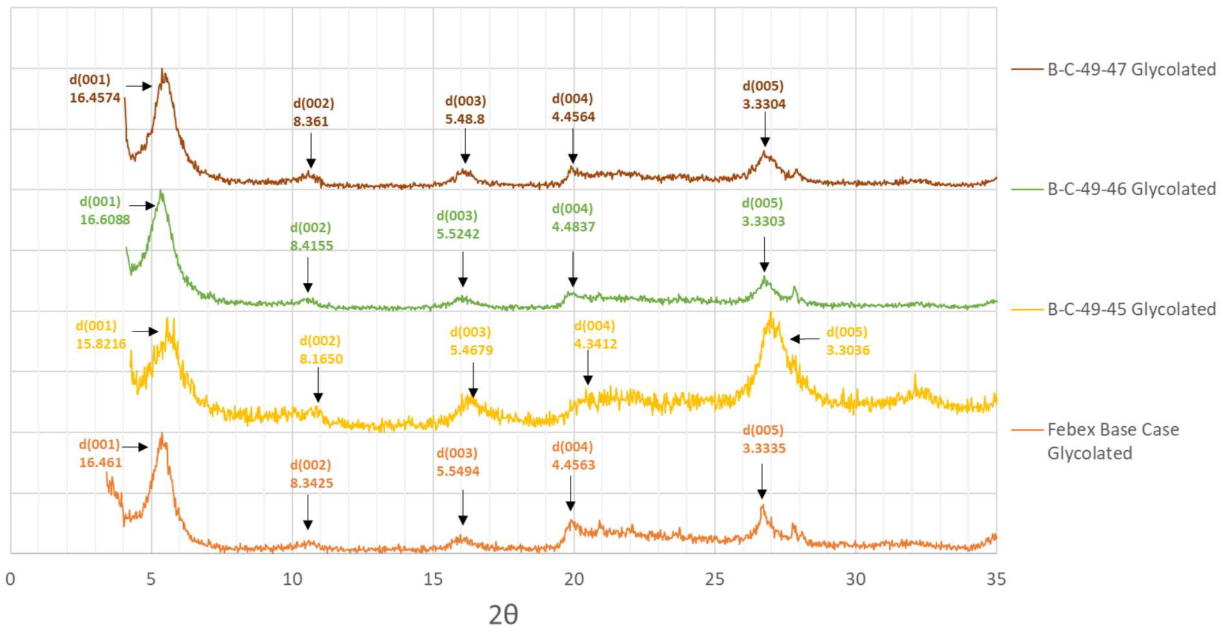

Figure 12. XRD spectra for various locations of B-C-49 block samples along with d-spacings (see schematic Fig. 3 for sample locations). XRD spectrum of FEBEX base case or reference material is shown at the bottom for comparison.

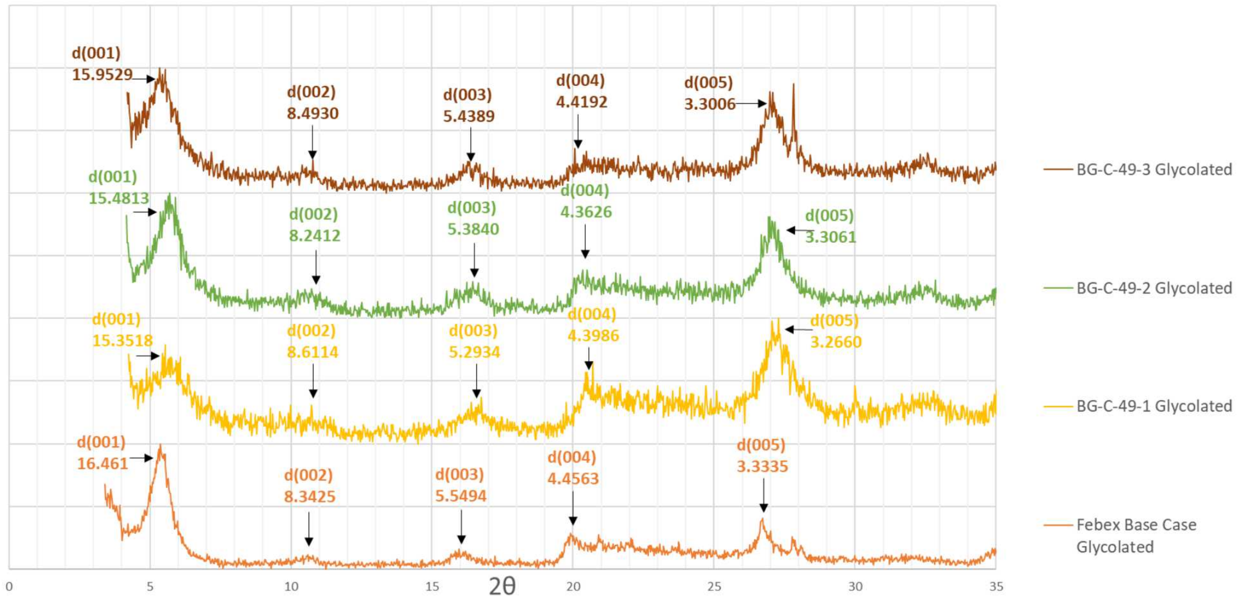

Figure 13. XRD spectra for various locations of BG-C-49 block samples along with d-spacings (see schematic Fig. 3 for sample locations). XRD spectrum of FEBEX base case or reference material is shown at the bottom for comparison. These are the most distal bentonite samples from the heater surface.

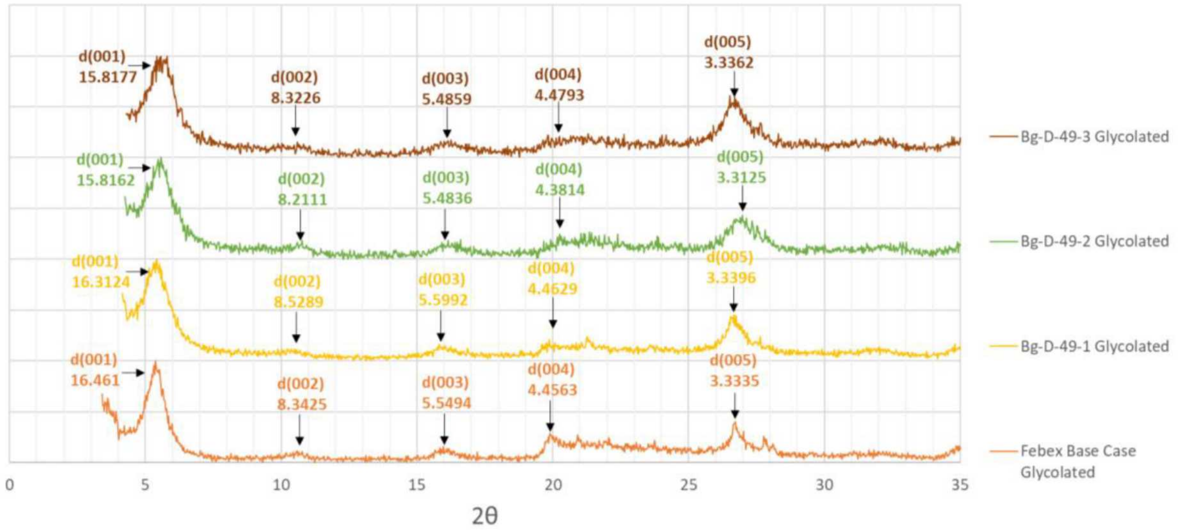

Figure 14. XRD spectra for various locations of BG-D-49 block samples along with d-spacings (see schematic Fig. 3 for sample locations). XRD spectrum of FEBEX base case or reference material is shown at the bottom for comparison. These are the most distal bentonite samples from the heater surface.

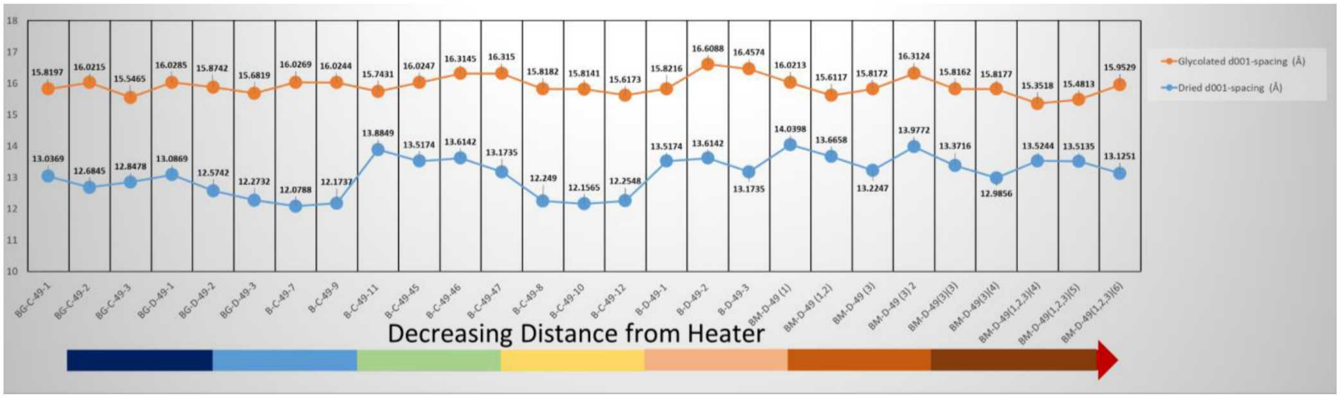

Figure 15. Distribution of d-spacing (d_{001}) (Å) values with distance from the heater for air-dried and glycolated bentonite samples (see schematic Fig. 3 for sample locations).

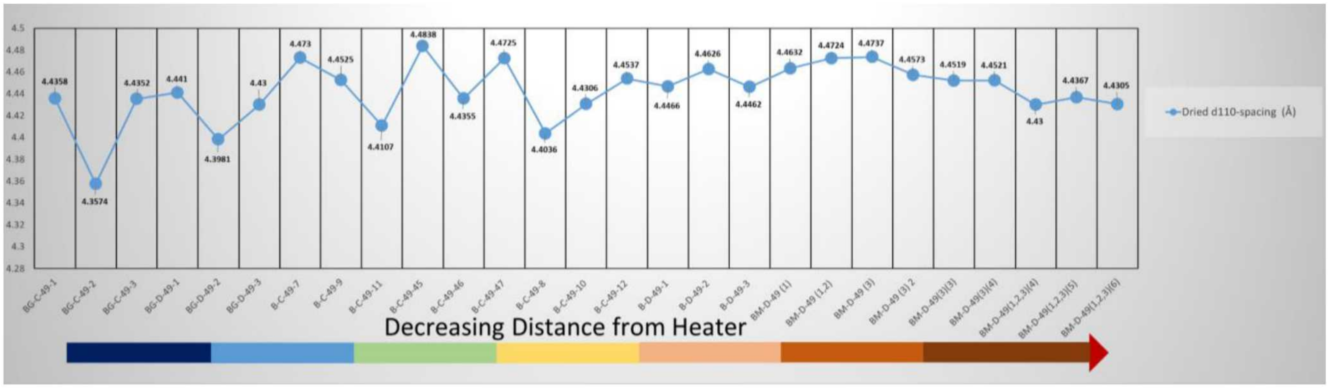

Figure 16. Distribution of d-spacing (d_{110}) (Å) values with distance from the heater for air-dried bentonite samples (see schematic Fig. 3 for sample locations). Notice the reduced variability in d_{110} values for samples closest to the heater.

Using the differences in d_{001} d-spacing data between air-dried and glycolated bentonite samples we estimated the apparent relative extent of swelling to evaluate the effect of distance from the heater. Fig. 17 illustrates the distribution of values for the relative extent of swelling for the various samples with distance from the heater. Like the distributions of d_{110} reflections, the variability in the relative extent of swelling appears to be reduced for bentonite closest to the heater where the overall variation ranges from around 15%-20% in the BM-D-49 samples. The overall variation in relative swelling for samples far from the heater was larger in the order of ~14%-32%. The highest estimate of relative swelling extent is around 32% for samples located farther from the gallery axis whereas samples closest to the heater the value is around 20%. The reason for this larger variability in swelling behavior with distance from the heater is currently a matter of further study. This behavior could be related to thermal effects on bentonite and/or changes in the smectite chemistry. Moreover, such a level of variation at the scale of the sample blocks could have implications to swelling heterogeneities and thus uncertainties in the extent of swelling predicted in coupled THMC models. The XRD study is still work in progress and further analysis of these data plus additional XRD analyses are planned for future work. Increasing the number of XRD analyses in all samples is needed to advance further comparisons on variability trends between different locations.

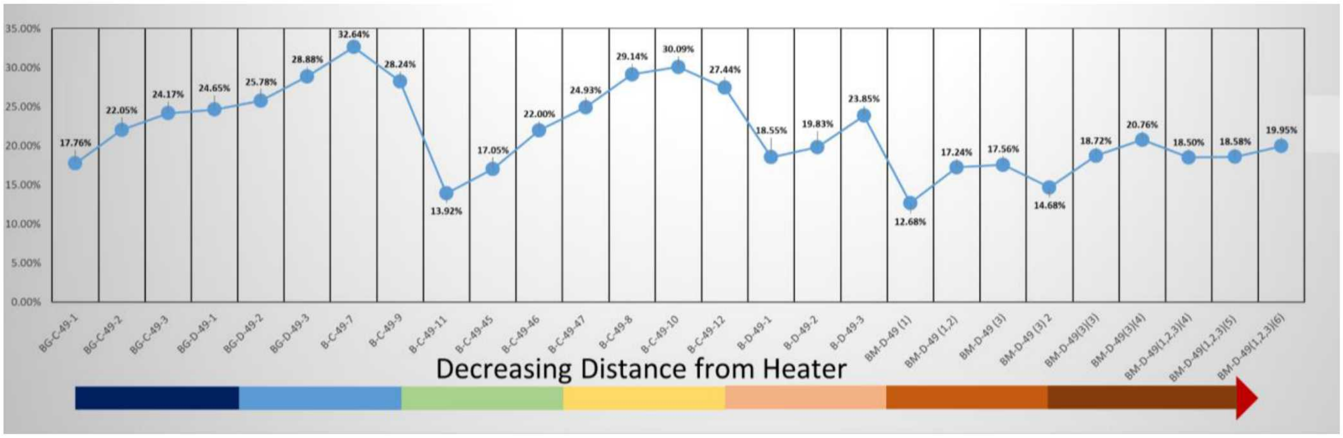

Figure 17. Distribution of estimated percent swelling with distance from the heater based in d-spacing measurements on air-dried and glycolated bentonite samples (see schematic Fig. 3 for sample locations). Notice the reduced variability in estimated swelling extent for samples closest to the heater.

V. DECOVALEX-2019 Task C: GREET (Groundwater REcovery Experiment in Tunnel), Mizunami URL, Japan

The DECOVALEX-2019 project phase started this year with seven tasks (A-G) targeting various issues relevant to coupled THMC processes driven experimental and URL field data. The Disposal in Argillite work package has expressed interest in the GREET (Groundwater REcovery Experiment in Tunnel, Mizunami URL, JAEA, Japan) URL project on the hydrochemical characterization of the site as part of the groundwater recovery activity from the closure test drift (CTD). The CTD is a tunnel section (46.5 m long × 5.0 m wide × 4.5 m high) of the URL sealed by plug and filled with groundwater. A series of boreholes allow for monitoring water pressure and chemistry during the experiment. In FY17, geochemical modeling was applied to the analysis of dilution trends observed in monitoring borehole data through simulation of groundwater mixing. Interactions with cementitious barrier materials in the CTD were evaluated through 1D reactive-transport modeling for a water-filled tunnel scenario. The current study extended the work conducted on cement interactions in the flooded CTD to evaluate shotcrete liner interactions using a 3D model representation of this domain implemented in the reactive transport simulation code PFLOTRAN. pH and Cl concentration data obtained recently at the site will be used as a test to the model.

The GREET project task leader has kindly provided web access to the geochemical and hydrological data, as it becomes available, to be reviewed by the task participants. Hydrochemical data from the DECOVALEX-19 (Task C) was obtained from the JAEA team and/or information at the GREET website (http://www.jaea.go.jp/04/tono/miu/dataset/greet/greet.html).

Closure Test Drift (CTD): 3D H-C Model of Shotcrete Liner Interactions and 12MI33 Monitoring Borehole

The Closure Test Drift (CTD) is a tunnel facility (Fig. 18) at 500 meters below ground level to investigate the effects of hydrological, geomechanical, and geochemical variations during drift excavation and post-closure in fractured granitic rock. The facility is equipped with monitoring probes for water sampling, hydraulic pressure, and rock displacement. Mapping of fractures was conducted during drift excavation. The CTD tunnel is lined with Mg-bearing ordinary Portland cement (OPC) shotcrete and is sealed by using a low-heat Portland cement plug (Iwatsuki et al., 2017). After closure, the tunnel was filled with water to study environmental changes including effects on hydrochemistry due to interactions with barrier materials such as the shotcrete. Like FEBEX-DP and other international repository science activities, interactions with cementitious barrier materials (e.g., shotcrete) is important given its potential for alkaline reactions with other silicates (e.g., clay barriers, host rock) and the generation of high pH pore solutions. These processes could lead to dissolution/precipitation processes at barrier interfaces that could affect solute (radionuclide) transport and clay barrier sorption properties.

A 3D reactive transport representation (Fig. 19) has been implemented on a hydrological model of the site near the CTD. The goal is to extend the hydrological to capture the extent of high pH effects within the flooded tunnel and with distance from the cement-water interface. Such interactions in the water-filled zone may influence pore solution chemistry in the nearby monitoring borehole (12MI33) where fractures in the excavated disturbed zone (EDZ) are present throughout the length of the CTD. Currently, the hydrological model does not include fractures but such features is planned for future work. Water chemistry measurements in zone 6 of the 12MI33 monitoring borehole show elevated pH values suggesting the influence of nearby cement liner material in the sampled solution.

The 3D reactive reactive-transport model implementation is done in PFLOTRAN using similar parameters (e.g., material properties) to those adopted previously in the 1D evaluation of EBS material interactions (Jové Colón et al., 2016). The PFLOTRAN simulations were conducted in TH mode (coupled thermal-hydrological flow) assuming full saturation and transport by diffusion only. Thermodynamic data for cementitious phases such as CSH(1.6), portlandite, and ettringite were obtained from the THERMODDEM database (Blanc et al., 2012; Blanc et al., 2006). The composition of the cementitious domain resembles that of ordinary Portland cement (OPC) assuming a calcite aggregate (Jové Colón et al., 2016). Dissolution rates of cementitious solids were obtained from various sources as described in Jové Colón et al. (2016). The length of water-filled domain is about 47 m with a height of 5 m closely resembling the CTD dimensions. The cement plug thickness is 2 m and the shotcrete liner is 0.1 m. The flooded CTD domain is represented by a porous medium having a porosity of almost unity and a very high permeability. The groundwater in the flooded domain is assumed to have the same chemistry as that of the host granitic rock. This groundwater also represents the starting solution chemistry of the filled CTD. The simulations were performed over a period of 400 days.

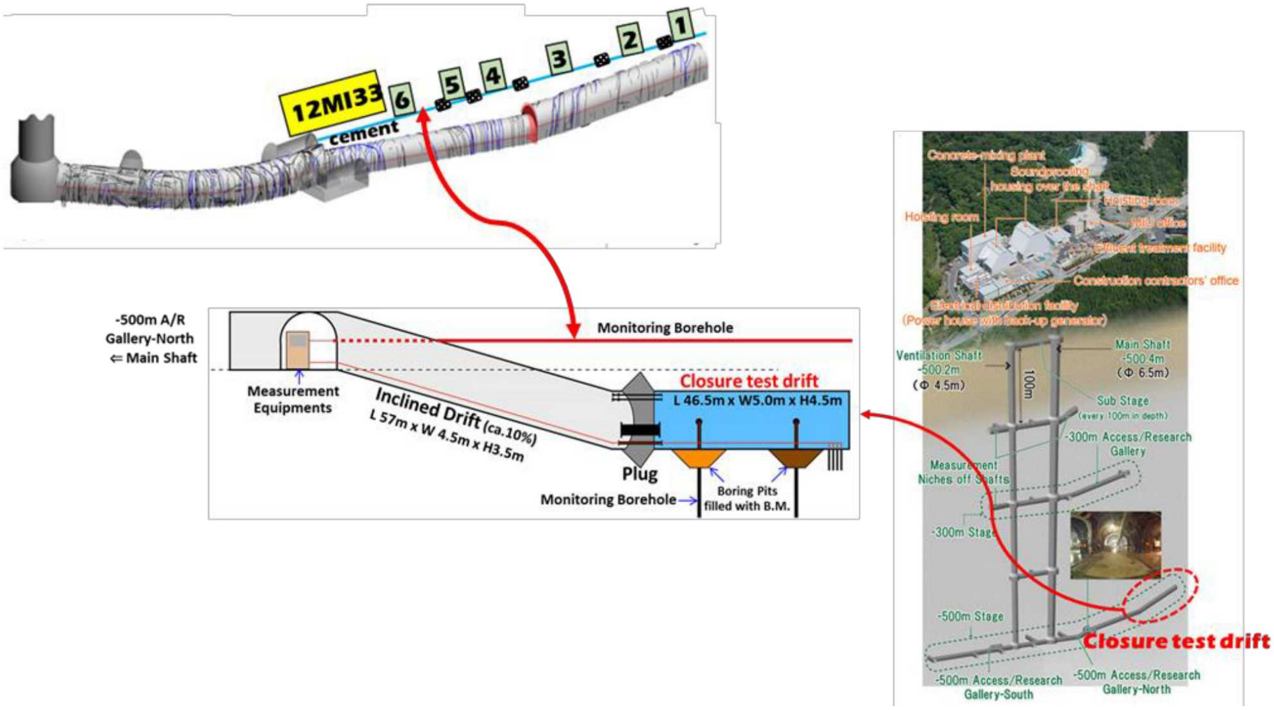

Figure 18. Diagrammatic picture of the closure test drift (CTD) at the Mizunami URL site, Japan. Upper schematic picture shows the inclined tunnel with CTD and the 12MI33 borehole with six monitoring zones. Figure content kindly provided by Dr. Teruki Iwatsuki (JAEA).

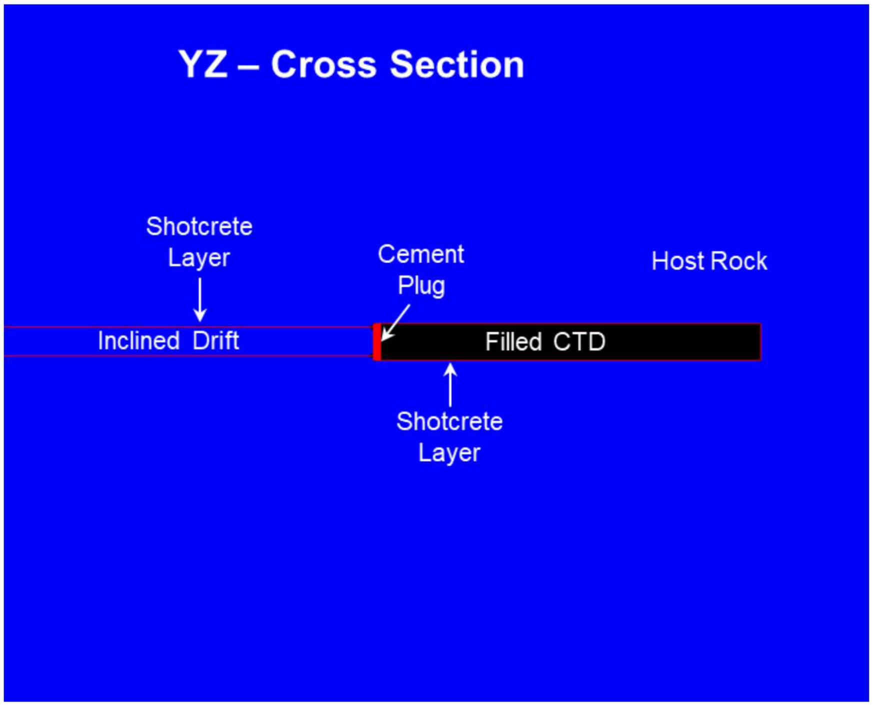

Figure 19. Schematic figure showing a YZ of the model domain in the PFLOTRAN reactive transport simulation of the CTD. Red areas delineate the shotcrete liner and cement plug. Observation points (not shown) are positioned at the tunnel length midpoint starting from the shotcrete-water interface up to a meter inside the water-filled tunnel.

Fig. 20 shows four time-snapshots (0, 70, 150, 310 days) of the pH mapping to represent the evolution of the reactive front from the shotcrete liner domain. As expected, pH increases with time from the interface into the water-filled CTD region and the host rock. After ~300 days of simulation time, the increase in pH because of the advancing front reaches ~0.5 m from the shotcrete interface into flooded CTD. About 1 m into the CTD, the pH remains close to the starting pH 8.9 for remainder of the simulation.

The current stage of GREET effort involves the prediction of changes in groundwater chemistry to then be compared with data from monitoring boreholes from within the CTD and from the host rock within the excavated disturbed zone (EDZ). Fig. 21 (upper panel) shows the pH predictions from PFLOTRAN and the JAEA group along with pH and Cl^- measurements of the solution within the CTD. The measured pH data (blue dots connected by a line) show a rapid monotonic increase early in time then progressing towards a pH~10. Notice that measure pH data after 3/2016 show more variation with time (i.e., deviations from a monotonic increase) but still trending towards pH~10. The PFLOTRAN simulation results (solid curves) are shown for three observation points at distance from the shotcrete interface (at the interface, 0.45 m, and 1 m) into the filled CTD. Notice that pH predictions at the interface overestimate the measured data progressing towards eventual equilibrium with the shotcrete cement (pH~11.3). As expected, predictions at 0.45 m show a slower pH increase due to diffusive transport from the shotcrete interface into the filled CTD. This increase reaches pH~10.3 towards the end of the simulation which is closer to the measured pH and it is also close to the JAEA Case 0 predictions. pH predictions at 1 m from the shotcrete interface show little increase with time indicating the limited effect of the reaction front on groundwater pH towards the tunnel axis. These predictions are also consistent with that of the JAEA Case 1.

Fig. 21 shows the measured concentration of Cl^- (lower panel) decreasing with time starting from 475 mg/L towards a steady-state value of ~403 mg/L. Although the PFLOTRAN simulation predicts a decrease in Cl^- concentration with time at the shotcrete interface, the extent of such is much smaller when compared to the measurement. It is not clear what would cause such a large decrease but possible reasons are groundwater mixing/dilution and/or Cl^- uptake by precipitation of a Cl-bearing cementitious phase. Both are possibilities that need verification through monitoring activities.

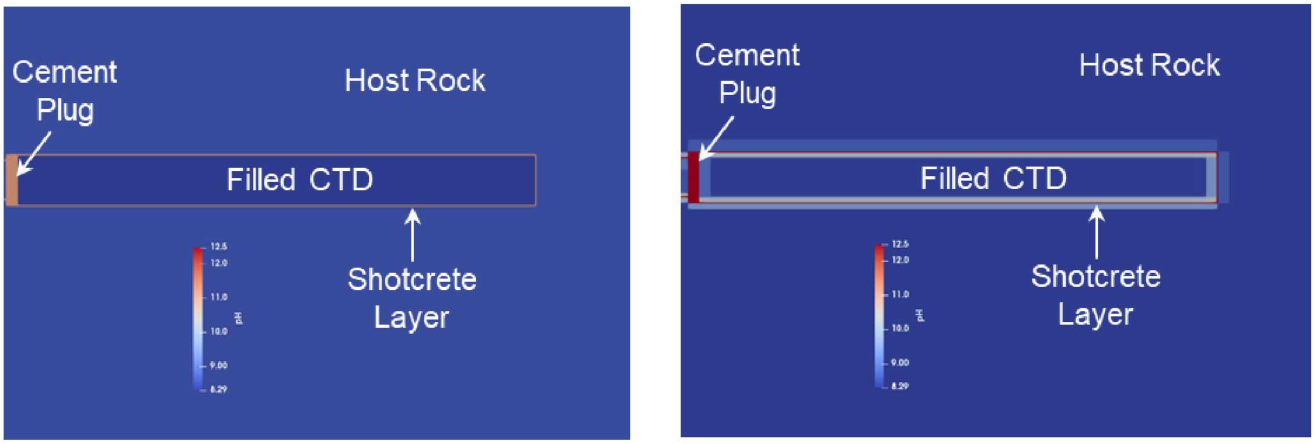

0 days *70 days*

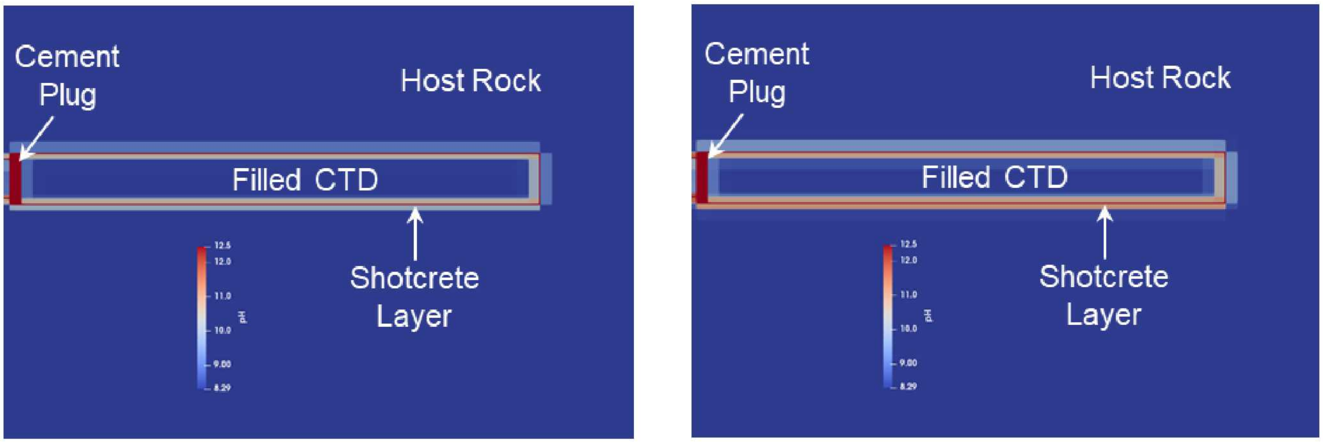

150 days *310 days*

Figure 20. Predicted pH of the PFLOTRAN 3D reactive transport model of the CTD and surrounding host rock. The reaction front diffuses into the CTD and into host rock.

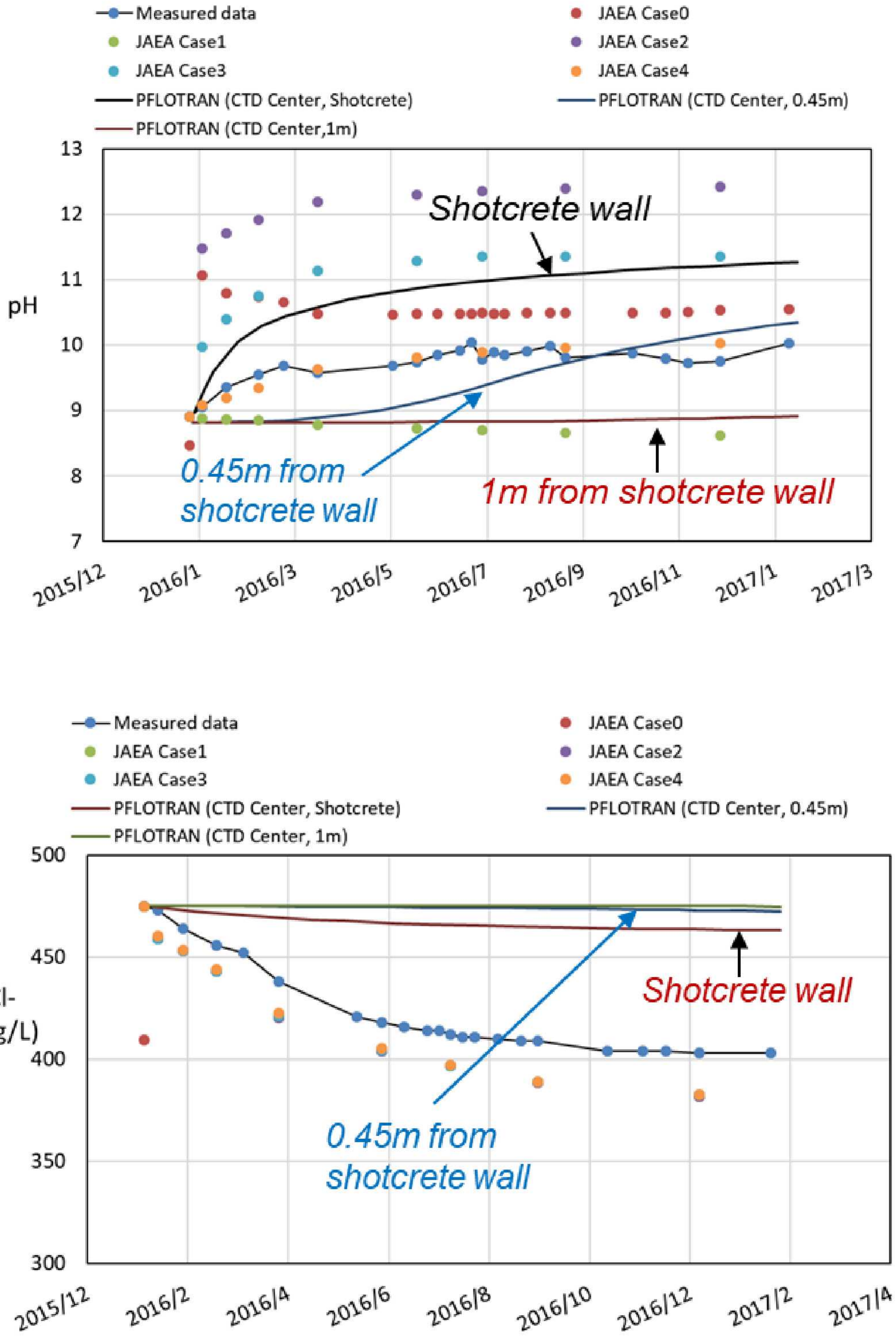

Figure 21. Measured and predicted pH (upper panel) and Cl$^-$ concentration (lower panel) profiles at the midpoint region of the CTD.

Fig. 22 describes measured and predicted pH at the six monitoring zones in borehole 12MI33. As illustrated in this figure, the monitoring borehole lies in the host rock parallel to the CTD and next to the inclined tunnel. The groundwater in this region interacts with the granitic host rock, however, zone 6 is closer to the cement lining. This is also illustrated in Fig. 22 where sampled groundwaters in zone 6 reaches pH~11. The PFLOTRAN pH prediction is the essentially the same for all six zones where this trend is generally consistent within the scatter of the measured pH's from zones 1-5. However, the prediction for zone 6 doesn't capture the pH increase most likely because of limited interaction with the cement liner. This may be indicative of enhanced transport in this particular zone and the next step will to accommodate this effect in the model.

All these preliminary results provide ideas on how to improve the 3D H-C model:

- Finer mesh at the shotcrete-water interface inside the filled CTD. This would allow the placement of observation points at shorter distances to monitor chemical changes away from the shotcrete interface.
- The initial rapid increase in measured pH is difficult to simulate in scenarios where observations are far from the shotcrete interface. Therefore, changes to the kinetic rate law and transport parameterization should be considered to better represent such pH profile. Parameter analysis within the mineral dissolution kinetics formulations in PFLOTRAN will be considered for dissolution cementitious phase (e.g., portlandite).
- Addition of Cl-bearing cementitious phases (e.g., Friedel's salt) to represent Cl^- depletion through solid formation. Groundwater mixing close to the shotcrete-rock domain will be explored as well.
- Shotcrete composition will be updated to capture the effects of Mg-bearing phases present in the liner material.
- Extending the 3D H-C model to accommodate fracture effects on flow and transport.

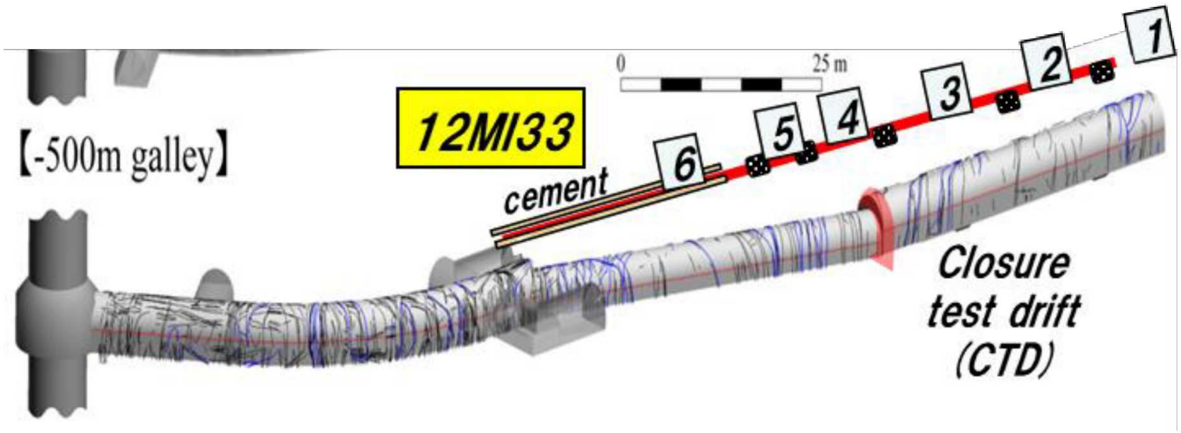

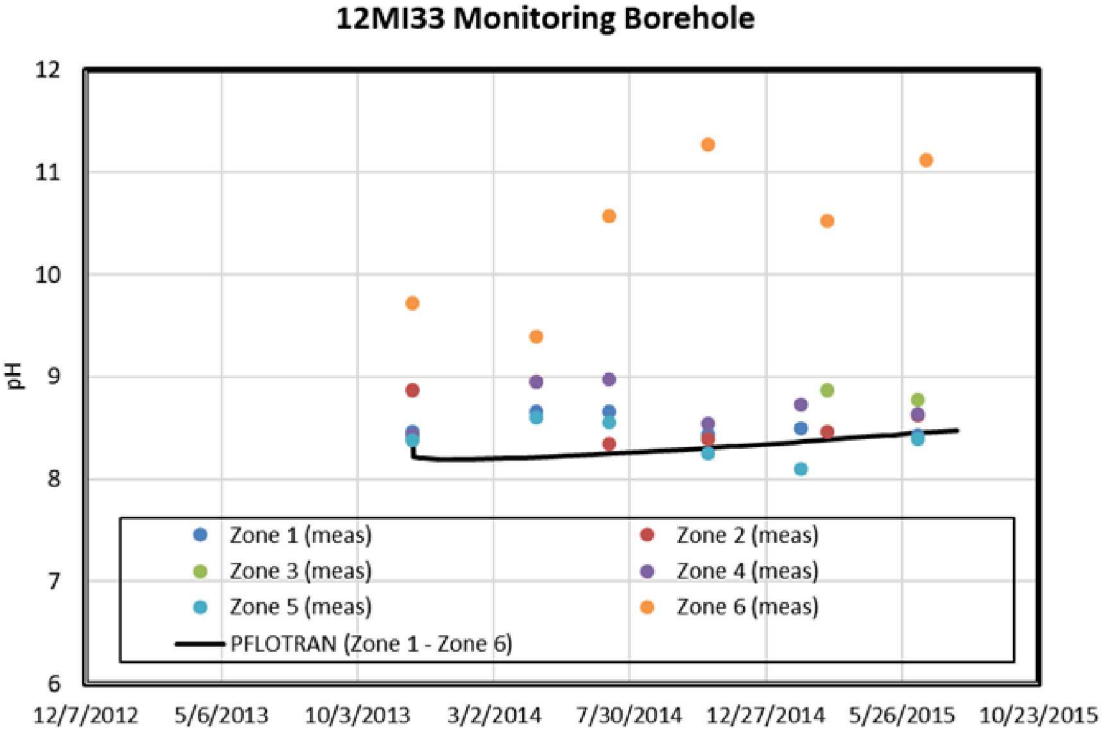

Figure 22. Schematic diagram of borehole 12MI33 (upper panel) with six monitoring zones. Measured and predicted pH (lower panel) profiles at monitoring zones 1 through 6.

VI. Conclusions

- **FEBEX-DP:** Compositional (XRF), structural (XRD), and thermal (TGA/DSC) characterization studies on FEBEX-DP bentonite samples from Section 49 were conducted to evaluate the effects thermal loads with distance from the heater. The most salient features of this characterization study can be summarized as follows:
    - XRF analyses revealed Mg enrichment in samples closest to the heater. This observation is corroborated with other FEBEX-DP studies in other sampled sections. This Mg enrichment is distinctly sharp for samples adjacent to the heater surface and may indicate thermally-induced effects of bentonite interactions driven by elevated temperatures. Such a change in smectite composition could potentially affect swelling behavior and sorption properties, and therefore its influence on barrier performance under thermal loads needs further investigation.
    - TGA/DSC thermal analyses indicate that measured water content falls within the data bounds of other FEBEX-DP studies from other sampled sections. There is a rather weak tendency towards higher water content with distance from the heater surface. Overall, TGA and DSC profiles with temperature are similar to those from other FEBEX-DP bentonite samples and literature studies on montmorillonite.
    - XRD spectra and d-spacing values for samples close and far from the heater are similar to others in the FEBEX-DP project. There is no clear trend or apparent correlation between d_{001} values and distance from the heater. Similarly, d_{110} values show no clear trend with distance from the heater. However, there is an apparent reduction in variability for d_{110} values for samples closest to the heater. Similarly, estimates of relative extent of swelling between air-dried and glycolated bentonite samples indicate a similar reduction in variability for samples closest to the heater. The swelling extent variability with distance from the heater appears to be significant and could have implications to the uncertainty in the prediction of swelling in response to thermal effects on bentonite.
- **DECOVALEX-2019 Task C of GREET Experiment** – 3D reactive transport modeling of the CTD and monitoring borehole 12MI33:
    - 3D reactive transport modeling of shotcrete liner interactions was implemented on a hydrological model of the site comprising the CTD. PFLOTRAN predictions of pH and Cl^- from groundwaters sampled at the midpoint length of the CTD showed deviations the measurements. The predicted pH overestimates the measured data at later times whereas the predicted Cl^- concentration prediction underestimates its decrease with time. Assessing the nature of these deviations is currently work in progress where future work will include exploring changes to kinetic rate law and transport parameters to better represent such pH profile. Groundwater mixing/dilution and/or Cl^- uptake by precipitation of a Cl-bearing phase (e.g., Friedel's salt) will be explored to explain the observed decrease in Cl^- concentration with time.
    - The 3D reactive transport model was also used to model groundwater interactions in six zones of the monitoring borehole 12MI33. This borehole lies parallel to the CTD and near the inclined drift. PFLOTRAN pH predictions of zones 1-5 in the monitoring borehole show overall consistency with the measured data indicating the control of the granitic host-rock on the groundwater chemistry. The pH in zone 6

appears to be influenced by interactions with the cement liner and could not be predicted by the current model. This probably suggest enhanced mixing at this zone.

VII. FY19 Work

Planned work on **FEBEX-DP** samples for FY19 (and the remainder of FY18):

- Continue assessment of compositional (XRF), structural (XRD), and thermal (TGS/DSC) data plus additional analyses of bentonite samples from Section 49. Focus on the evaluation of thermal analysis and XRD data with the observed compositional changes, and comparison with other studies on bentonite clay.
- Conduct compositional, structural, and thermal characterization of the FEBEX-DP bentonite samples from Section 58. This suite of samples is located far from the heater (in contrast with those of Section 49) and were not exposed to thermal loads.
- Experimental investigations on illitization using FEBEX-DP samples instead of treated clays as starting material. This work will be conducted in concert with the SFWST crystalline work package.

Planned work on **DECOVALEX Task C** for FY19 (and the remainder of FY18):

- Continue reactive-transport modeling work on DECOVALEX-2019 Task C (GREET) emphasizing on modeling the CTD chemical data. The effects of shotcrete liner interactions in the CTD will be the focus of this work to evaluate predictions of measured pH and Cl data. Shotcrete chemistry will be expanded to have Mg-bearing components instead of generic OPC.
- Expand reactive transport modeling to be integrated with hydrological simulations in fractured rock conducted with the SFWST crystalline work package team. Investigate the effect of fractures adjacent to monitoring boreholes on groundwater pH and other aqueous constituents.

VIII. References

Birkholzer, J., Faybishenko, B., Zheng, L., Rutqvist, J., Dobson, P., Fox, P.M., Reimus, P., Viswanathan, H., Jove-Colon, C.F., Wang, Y., Kuhlman, K., McMahon, K. and Zavarin, M., 2017. International Collaboration Activities in Different Geologic Disposal Environments (SFWD-SFWST-2017-000013), Prepared for US Department of Energy, Spent Fuel and Waste Disposition Campaign (SFWD-SFWST-2017-000013). (National Laboratory Report No. LBNL-2001063), Berkeley, California, pp. 236 pp.

Birkholzer, J., Faybishenko, B., Zheng, L., Rutqvist, J., Reimus, P., Viswanathan, H., Jove Colon, C.F., Wang, Y. and Zavarin, M., 2016. International Collaboration Activities in Different Geologic Disposal Environments (FCRD-UFD-2016-000077), Lawrence Berkeley National Laboratory (LBNL-1006321), Berkeley, CA USA.

Blanc, P., Lassin, A., Piantone, P., Azaroual, M., Jacquemet, N., Fabbri, A. and Gaucher, A., 2012. Thermoddem: A geochemical database focused on low temperature water/rock interactions and waste materials. Applied Geochemistry, 27: 2107-2116.

Blanc, P., Piantone, P., Lassin, A. and Burnol, A., 2006. Thermochimie : Sélection de constantes thermodynamiques pour les éléments majeurs, le plomb et le cadmium, Rapport final BRGM/RP-54902-FR. BRGM, France, pp. 157.

García-Siñeriz, J.L., Abós, H., Martínez, V., De la Rosa, C., Mäder, U. and Kober, F., 2016. FEBEX DP: Dismantling of heater 2 at the FEBEX "in situ" test: Description of operations - Arbeitsbericht NAB 16-11, National Cooperative for the Disposal of Radioactive Waste (NAGRA), Wettingen, Switzerland.

Grim, R.E., 1968. Clay mineralogy. International series in the earth and planetary sciences. McGraw-Hill, New York.

Huertas, F., Fuentes-Cantillana, J.L., Jullien, F., Rivas, P., Linares, J., Fariña, P., Ghoreychi, M., Jockwer, N., Kickmaier, W., Martínez, M.A., Samper, J., Alonso, E. and Elorza, F.J., 2000. Full-scale engineered barriers experiment for a deep geological repository for high-level radioactive waste in crystalline host rock (FEBEX project): Final report. EUR 19147, European Commission, Brussels.

Iwatsuki, T., Furue, R., Mie, H., Ioka, S. and Mizuno, T., 2005. Hydrochemical baseline condition of groundwater at the Mizunami underground research laboratory (MIU). Applied geochemistry, 20(12): 2283-2302.

Iwatsuki, T., Hagiwara, H., Ohmori, K., Munemoto, T. and Onoe, H., 2015. Hydrochemical disturbances measured in groundwater during the construction and operation of a large-scale underground facility in deep crystalline rock in Japan. Environmental Earth Sciences, 74(4): 3041-3057.

Iwatsuki, T., Munemoto, T., Kubota, M., Hayashida, K. and Kato, T., 2017. Characterization of rare earth elements (REEs) associated with suspended particles in deep granitic groundwater and their post-closure behavior from a simulated underground facility. Applied Geochemistry, 82: 134-145.

Jové Colón, C.F., Hammond, G.E., Kuhlman, K., Zheng, L., Kim, K., Xu, H., Rutqvist, J., Caporuscio, F.A., Norskog, K.E., Maner, J., Palaich, S., Cheshire, M., Zavarin, M., Wolery, T.J., Atkins-Duffin, C., Jerden, J.L., Copple, J.M., Cruse, T. and Ebert, W.L., 2016. Evaluation of Used Fuel Disposition in Clay-Bearing Rock (FCRD-UFD-2016-000074), Sandia National Laboratories, Albuquerque, NM. SAND2016-10311 R.

Martinez, V., Abós, H. and García-Siñeriz, J.L., 2016. FEBEXe: Final Sensor Data Report (FEBEX "in situ" Experiment) - Arbeitsbericht NAB 16-19, National Cooperative for the Disposal of Radioactive Waste (NAGRA), Wettingen, Switzerland.

Marty, N.C.M., Bildstein, O., Blanc, P., Claret, F., Cochepin, B., Gaucher, E.C., Jacques, D., Lartigue, J.E., Liu, S.H., Mayer, K.U., Meeussen, J.C.L., Munier, I., Pointeau, I., Su, D.Y. and Steefel, C.I., 2015. Benchmarks for multicomponent reactive transport across a cement/clay interface. Computational Geosciences, 19(3): 635-653.

McKay, J., 1992. Clay Separation. LSIS Technical Memorandum #92-1. University of Western Ohio.

Missana, T. and García-Gutiérrez, M., 2007. Adsorption of bivalent ions (Ca (II), Sr (II) and Co (II)) onto FEBEX bentonite. Physics and Chemistry of the Earth, Parts A/B/C, 32(8): 559-567.

Muurinen, A., 2011. Measurements on Cation Exchange Capacity of Bentonite in the Long-Term Test of Buffer Material (LOT), Working Report 2011-10. POSIVA, Eurajoki, Finland, pp. 30.

Tajeddine, L., Gailhanou, H., Blanc, P., Lassin, A., Gaboreau, S. and Vieillard, P., 2015. Hydration–dehydration behavior and thermodynamics of MX-80 montmorillonite studied using thermal analysis. Thermochimica Acta, 604: 83-93.

Teich-McGoldrick, S.L., Greathouse, J.A., Jové-Colón, C.F. and Cygan, R.T., 2015. Swelling Properties of Montmorillonite and Beidellite Clay Minerals from Molecular Simulation: Comparison of Temperature, Interlayer Cation, and Charge Location Effects. The Journal of Physical Chemistry C, 119(36): 20880-20891.

Vieillard, P., Tajeddine, L., Gailhanou, H., Blanc, P. and Lassin, A., 2016. Thermo-Analytical Techniques on MX-80 Montmorillonite: A Way to Know the Behavior of Water and its Thermodynamic Properties during Hydration–Dehydration Processes. Pharm Anal Acta, 7: 462.

Villar, M.V., Fernandez, A.M., Romero, E., Dueck, A., Cuevas, J., Plotze, M., Kaufhold, S., Dohrmann, R., Iglesias, R.J., Sakaki, T., Voltolini, M., Zheng, L., Kawamoto, K. and Kober, F., 2017. FEBEX-DP Post-mortem THM/THG Analysis Report, NAGRA Arbeitsbericht NAB 16-17. NAGRA, Wettingen, Switzerland, pp. 187 pp.

Wilson, J.C., Benbow, S., Sasamoto, H., Savage, D. and Watson, C., 2015. Thermodynamic and fully-coupled reactive transport models of a steel-bentonite interface. Applied Geochemistry.

Xie, M.L., Mayer, K.U., Claret, F., Alt-Epping, P., Jacques, D., Steefel, C., Chiaberge, C. and Simunek, J., 2015. Implementation and evaluation of permeability-porosity and tortuosity-porosity relationships linked to mineral dissolution-precipitation. Computational Geosciences, 19(3): 655-671.

IX. APPENDIX A

Complementary XRF and XRD Data

FEBEX-DP Bentonite Samples – Section 49

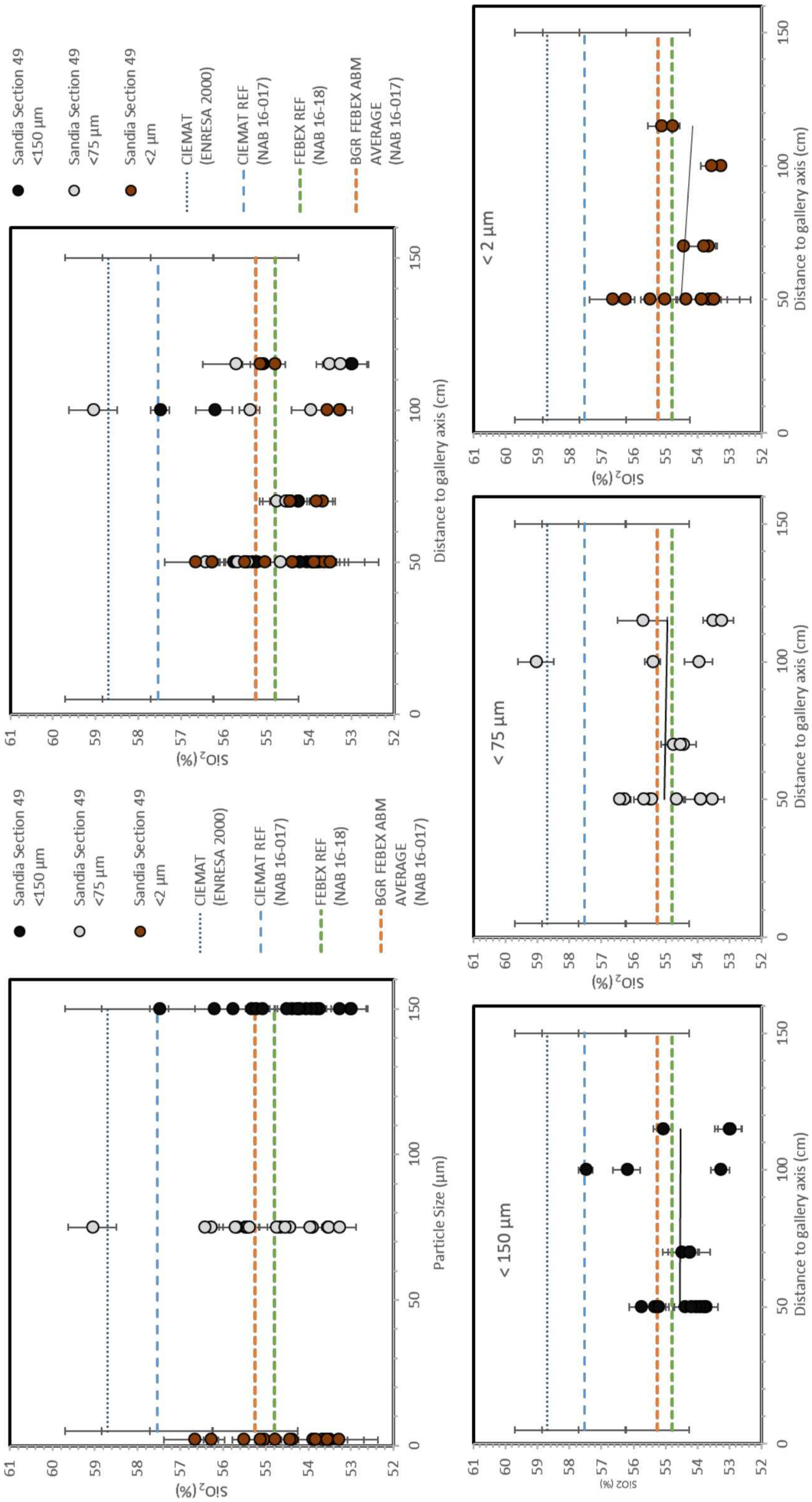

Figure A-1. Bulk bentonite XRF analyses of SiO_2 content for Section 49 samples as a function of distance from the gallery axis and particle size. Filled symbols denote analyses conducted in this study for size fractions of <150, <75, and <2 microns. Horizontal dashed-lines delineate the range of FEBEX bentonite compositions including reference values by different groups (Villar et al. 2017).

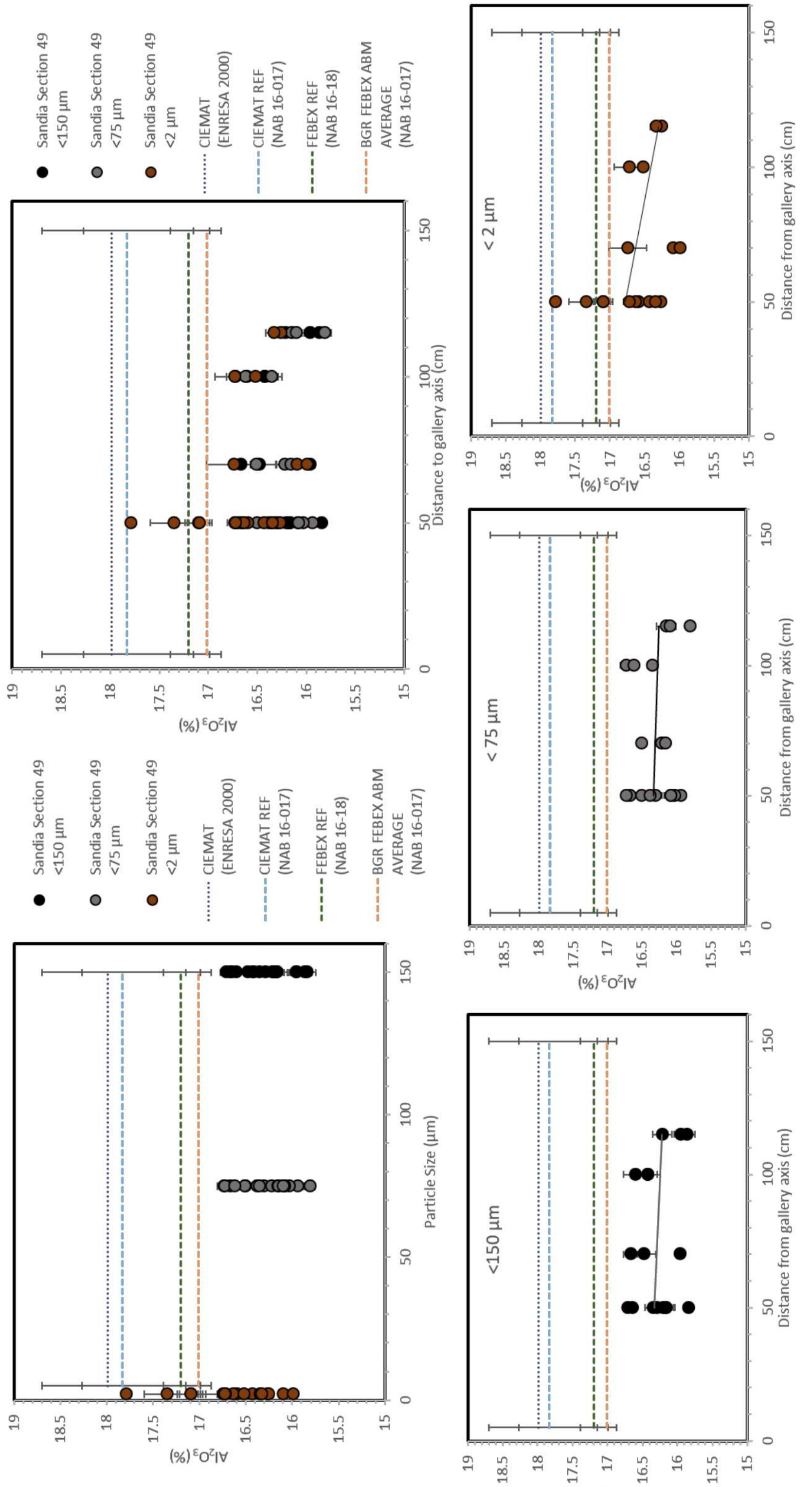

Figure A-2. Bulk bentonite XRF analyses of Al_2O_3 content for Section 49 samples as a function of distance from the gallery axis and particle size. Filled symbols denote analyses conducted in this study for size fractions of <150, <75, and <2 microns. Horizontal dashed-lines delineate the range of FEBEX bentonite compositions including reference values by different groups (Villar et al. 2017).

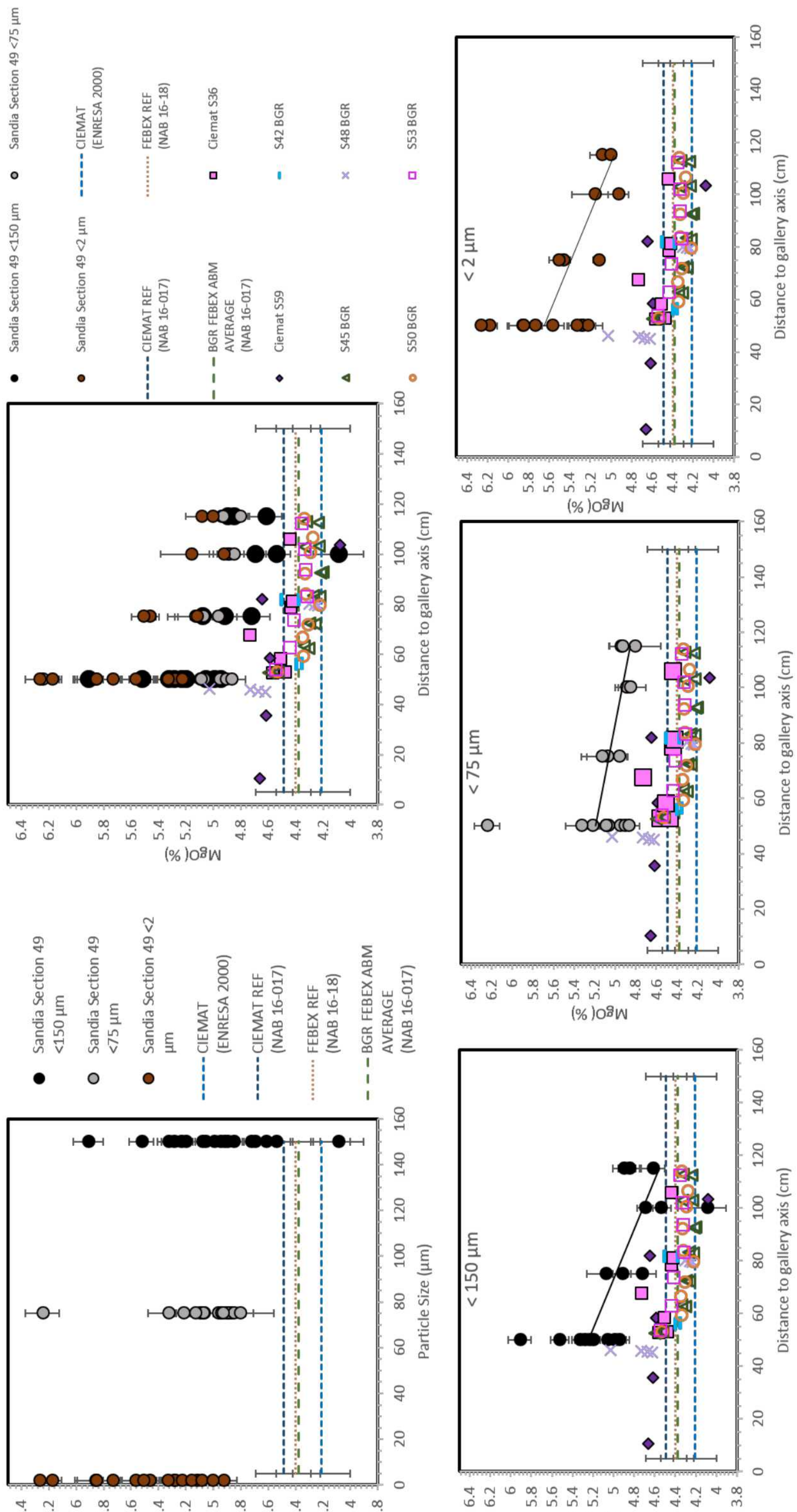

Figure A-3. Bulk bentonite XRF analyses of MgO contents for Section 49 samples as a function of distance from the gallery axis and particle size. Filled circles denote analyses conducted in this study for size fractions of <150, <75, and <2 microns. Horizontal dashed-lines delineate the range of FEBEX bentonite compositions including reference values by different groups (Villar et al. 2017).

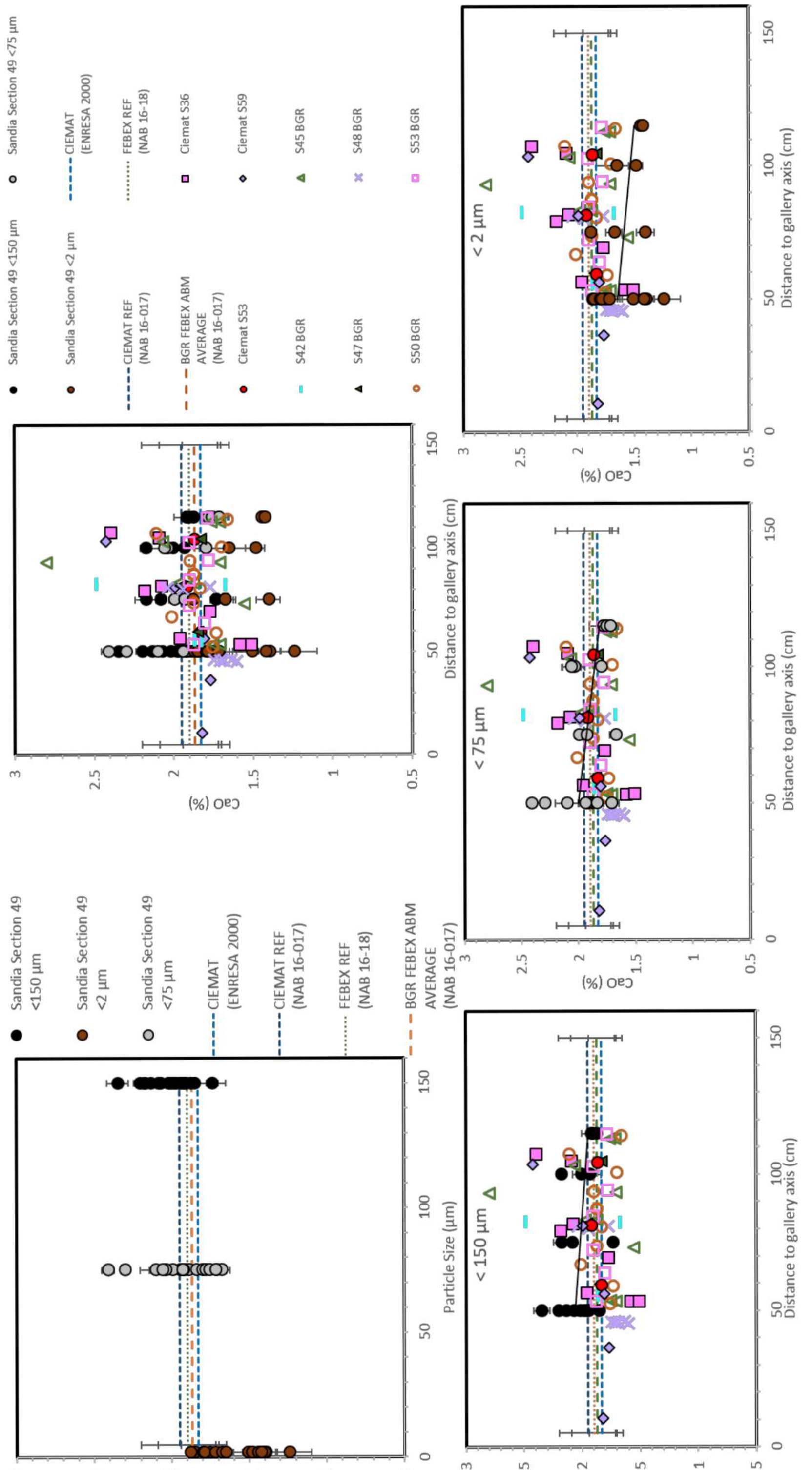

Figure A-4. Bulk bentonite XRF analyses of CaO contents for Section 49 samples as a function of distance from the gallery axis and particle size. Filled circles denote analyses conducted in this study for size fractions of <150, <75, and <2 microns. Horizontal dashed-lines delineate the range of FEBEX bentonite compositions including reference values by different groups (Villar et al. 2017).

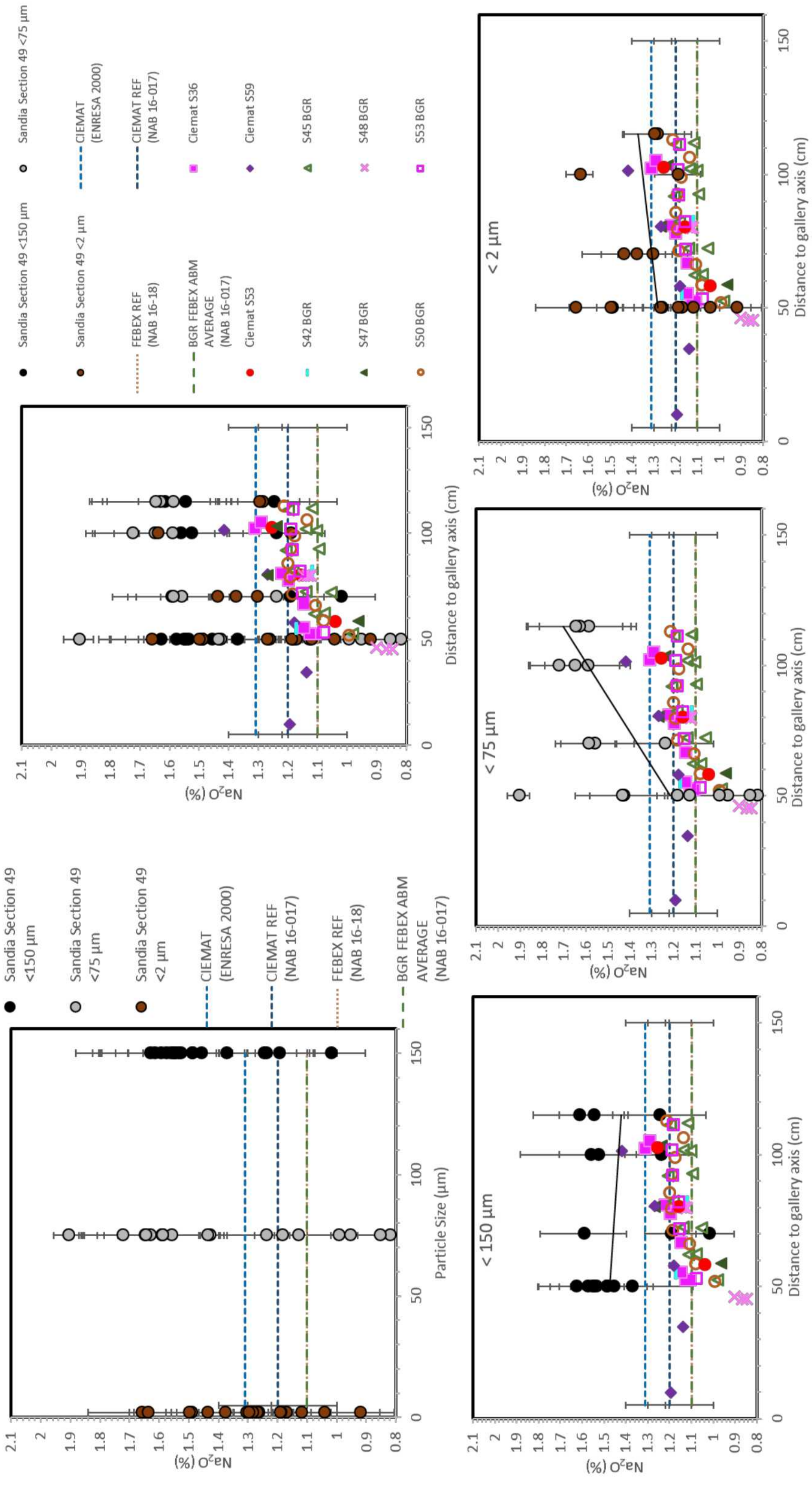

Figure A-5. Bulk bentonite XRF analyses of Na_2O contents for Section 49 samples as a function of distance from the gallery axis and particle size. Filled circles denote analyses conducted in this study for size fractions of <150, <75, and <2 microns. Horizontal dashed-lines delineate the range of FEBEX bentonite compositions including reference values by different groups (Villar et al. 2017).

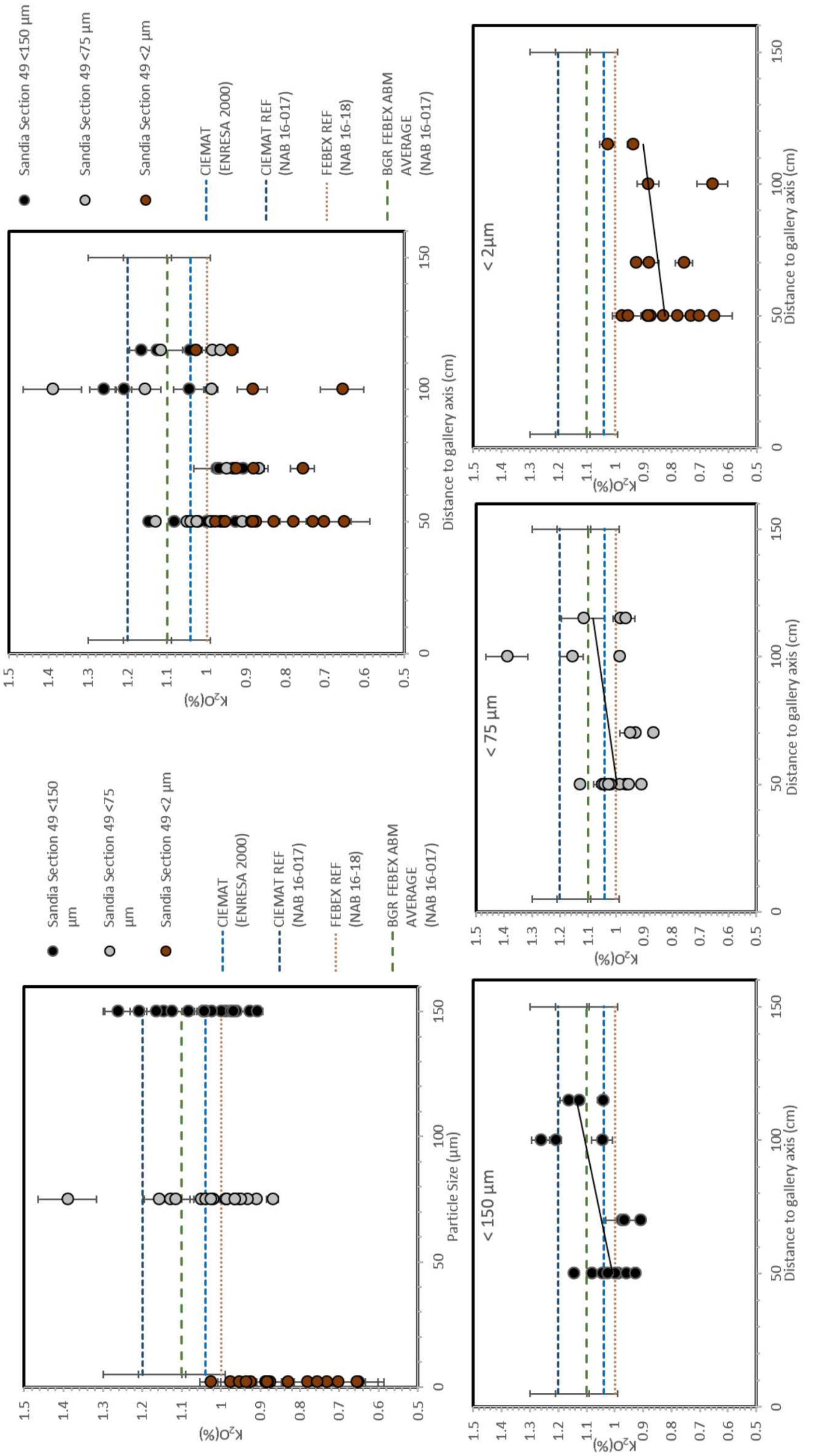

Figure A-6. Bulk bentonite XRF analyses of K_2O contents for Section 49 samples as a function of distance from the gallery axis and particle size. Filled circles denote analyses conducted in this study for size fractions of <150, <75, and <2 microns. Horizontal dashed-lines delineate the range of FEBEX bentonite compositions including reference values by different groups (Villar et al. 2017).

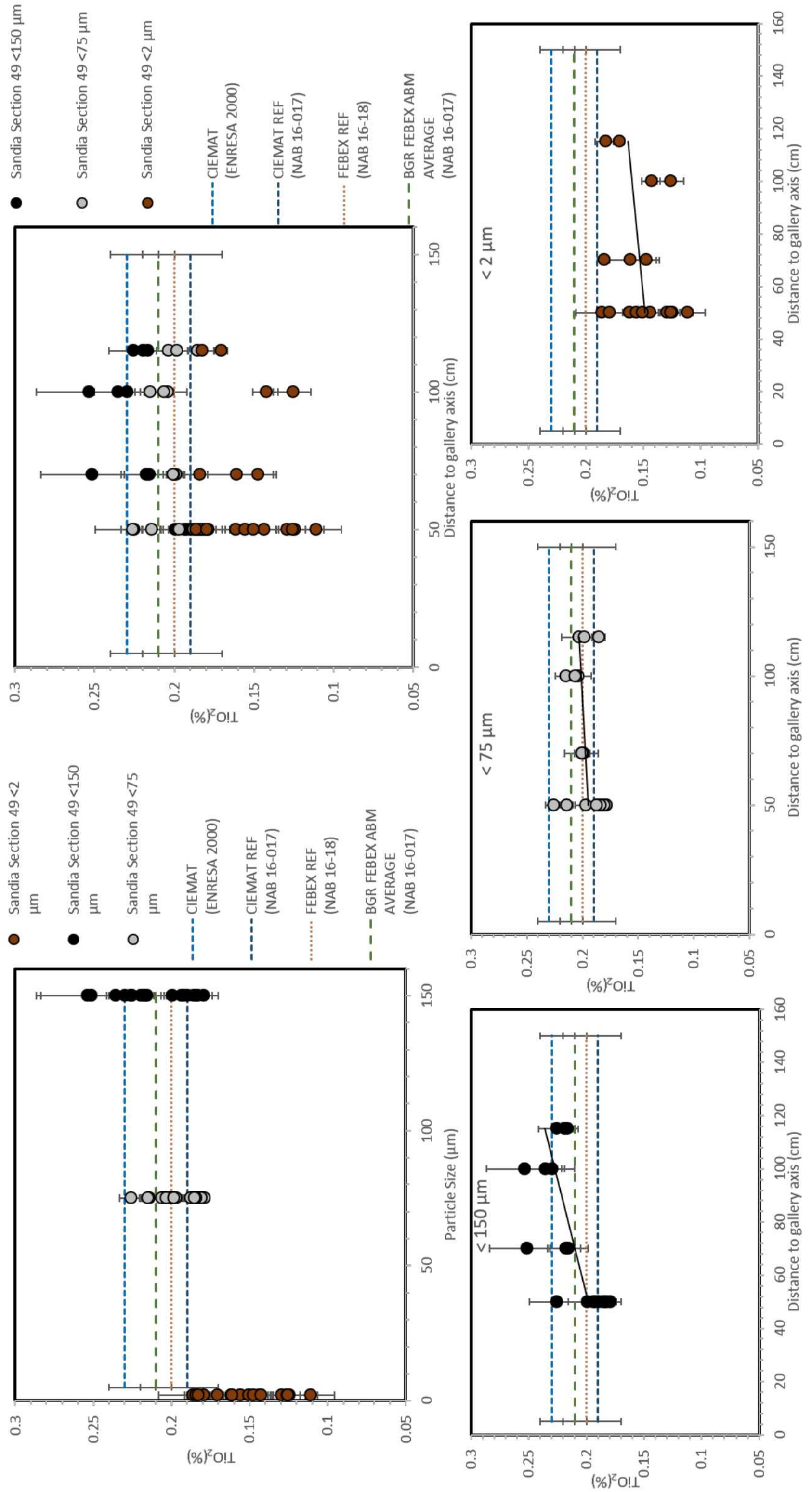

Figure A-7. Bulk bentonite XRF analyses of Ti_2O contents for Section 49 samples as a function of distance from the gallery axis and particle size. Filled circles denote analyses conducted in this study for size fractions of <150, <75, and <2 microns. Horizontal dashed-lines delineate the range of FEBEX bentonite compositions including reference values by different groups (Villar et al. 2017).

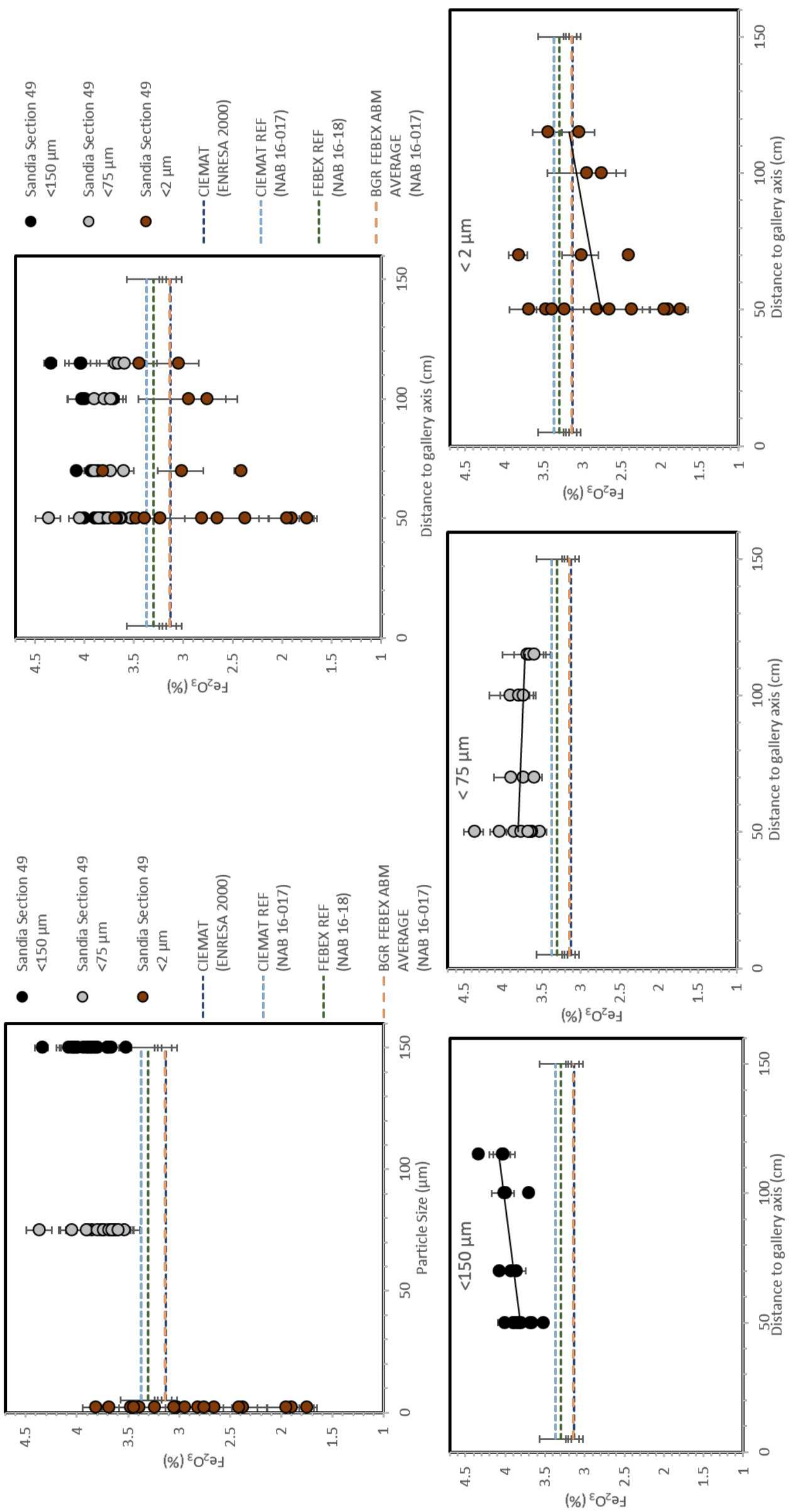

Figure A-8. Bulk bentonite XRF analyses of Fe_2O_3 contents for Section 49 samples as a function of distance from the gallery axis and particle size. Filled circles denote analyses conducted in this study for size fractions of <150, <75, and <2 microns. Horizontal dashed-lines delineate the range of FEBEX bentonite compositions including reference values by different groups (Villar et al. 2017).

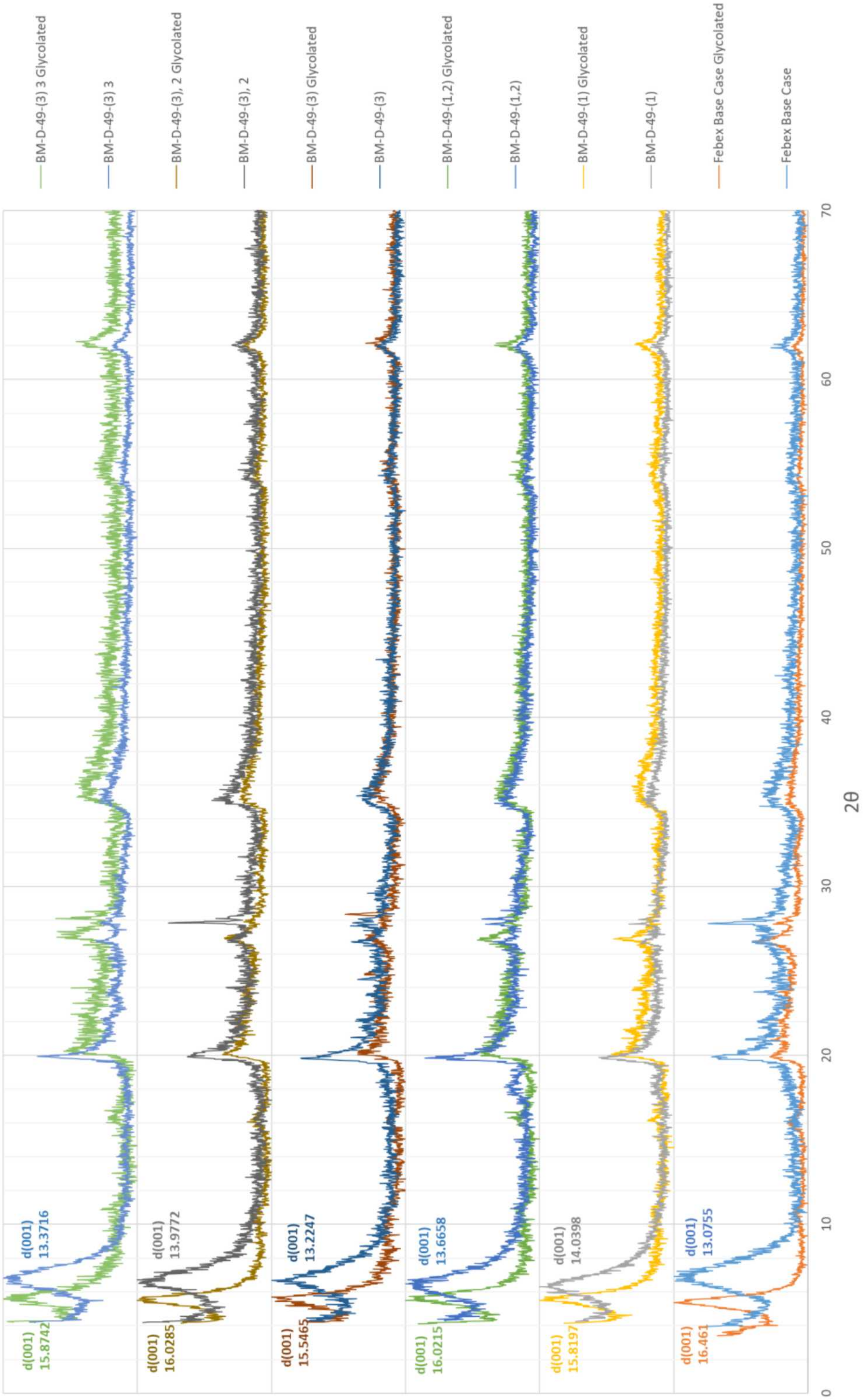

Figure A-9. XRD spectra (air-dried and glycolated) for various positions of BM-D-49 samples in the same blocks along with d-spacings (see schematic Fig. 3 for sample locations). XRD spectrum of FEBEX base case or reference material is shown at the bottom for comparison. These samples are closest to the heater.

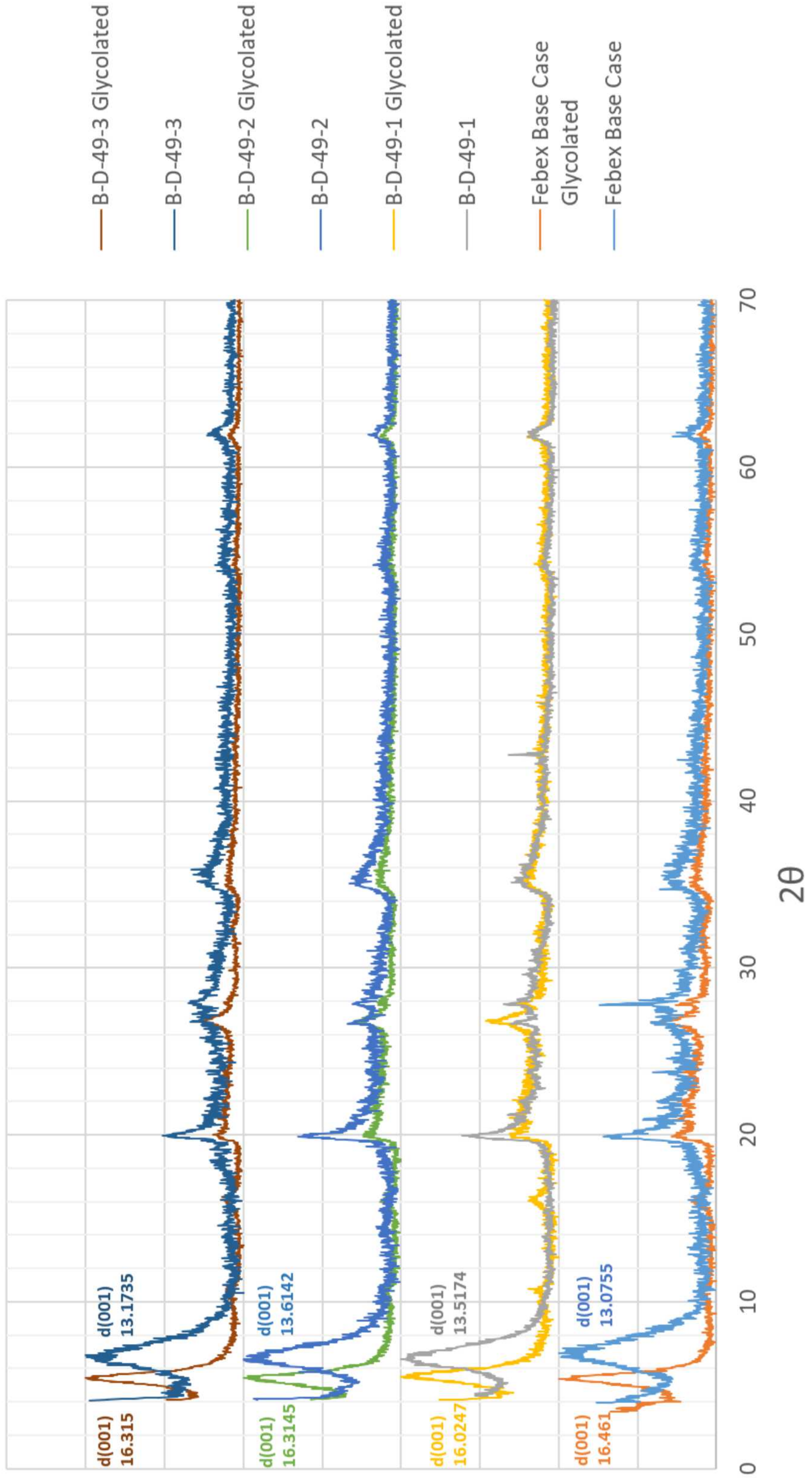

Figure A-10. XRD spectra (air-dried and glycolated) for various positions of B-D-49 samples in the same blocks along with d-spacings (see schematic Fig. 3 for sample locations). XRD spectrum of FEBEX base case or reference material is shown at the bottom for comparison.

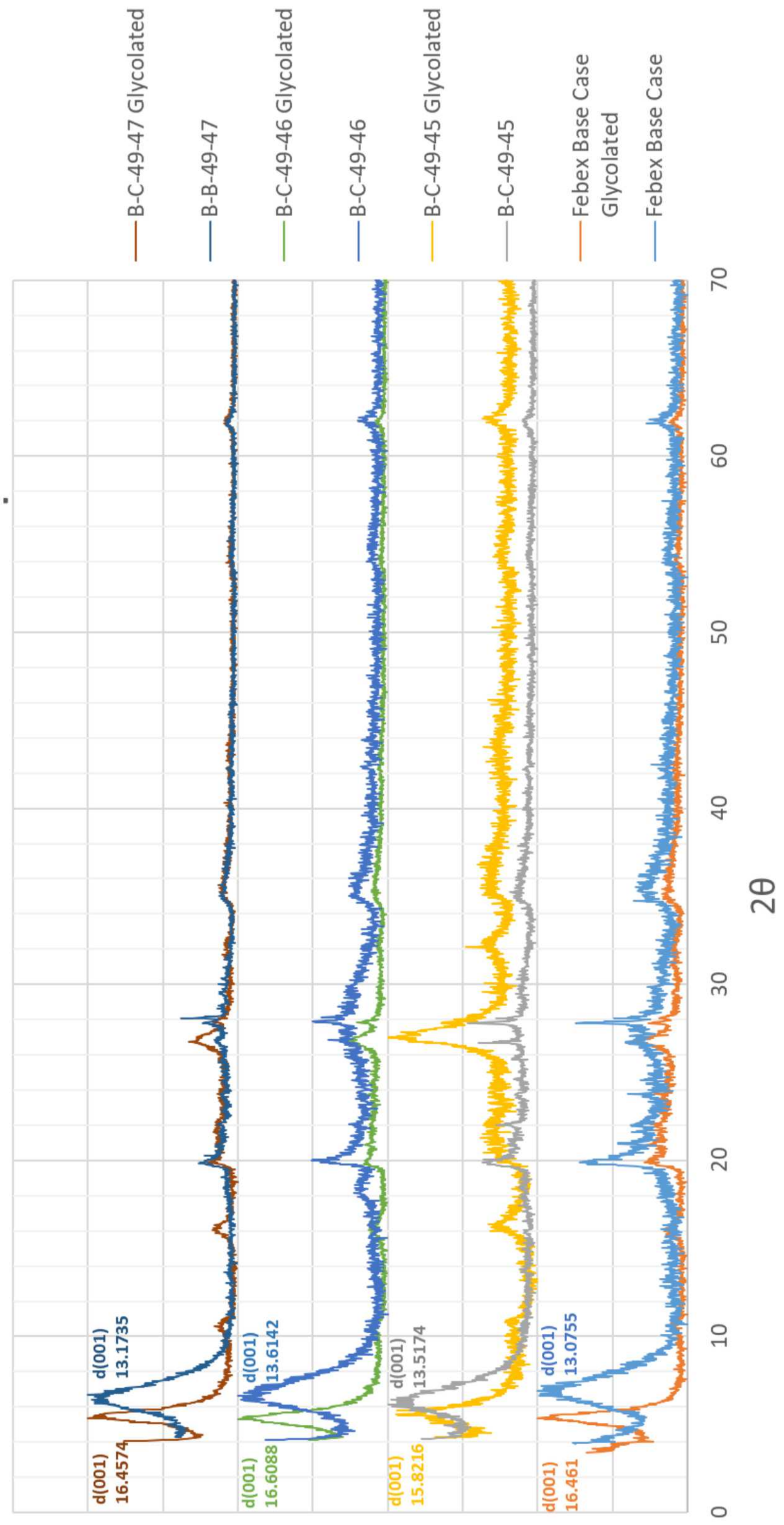

Figure A-11. XRD spectra (air-dried and glycolated) for various positions of B-C-49 samples in the same blocks along with d-spacings (see schematic Fig. 3 for sample locations). XRD spectrum of FEBEX base case or reference material is shown at the bottom for comparison.

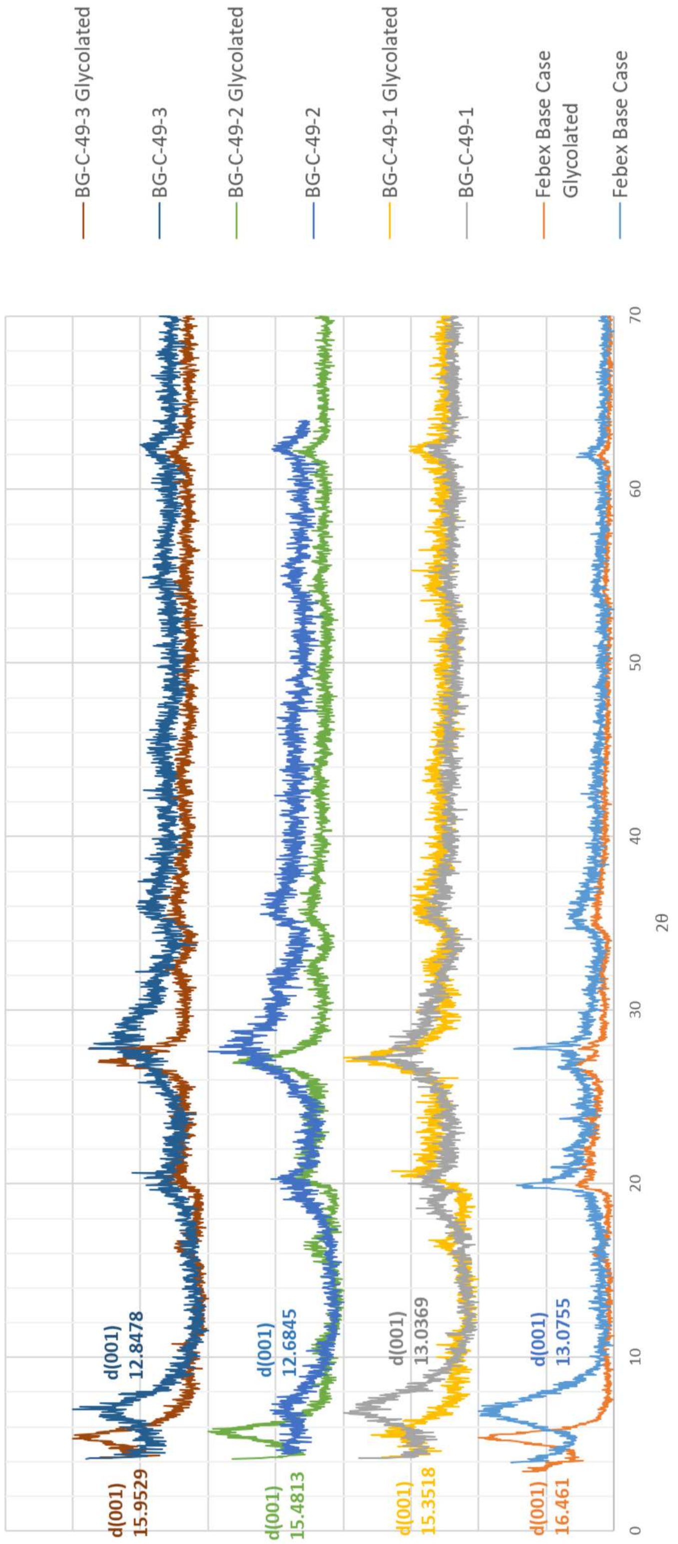

Figure A-12. XRD spectra (air-dried and glycolated) for various positions of BG-C-49 samples in the same blocks along with d-spacings (see schematic Fig. 3 for sample locations). XRD spectrum of FEBEX base case or reference material is shown at the bottom for comparison. These are the most distal bentonite samples from the heater surface.

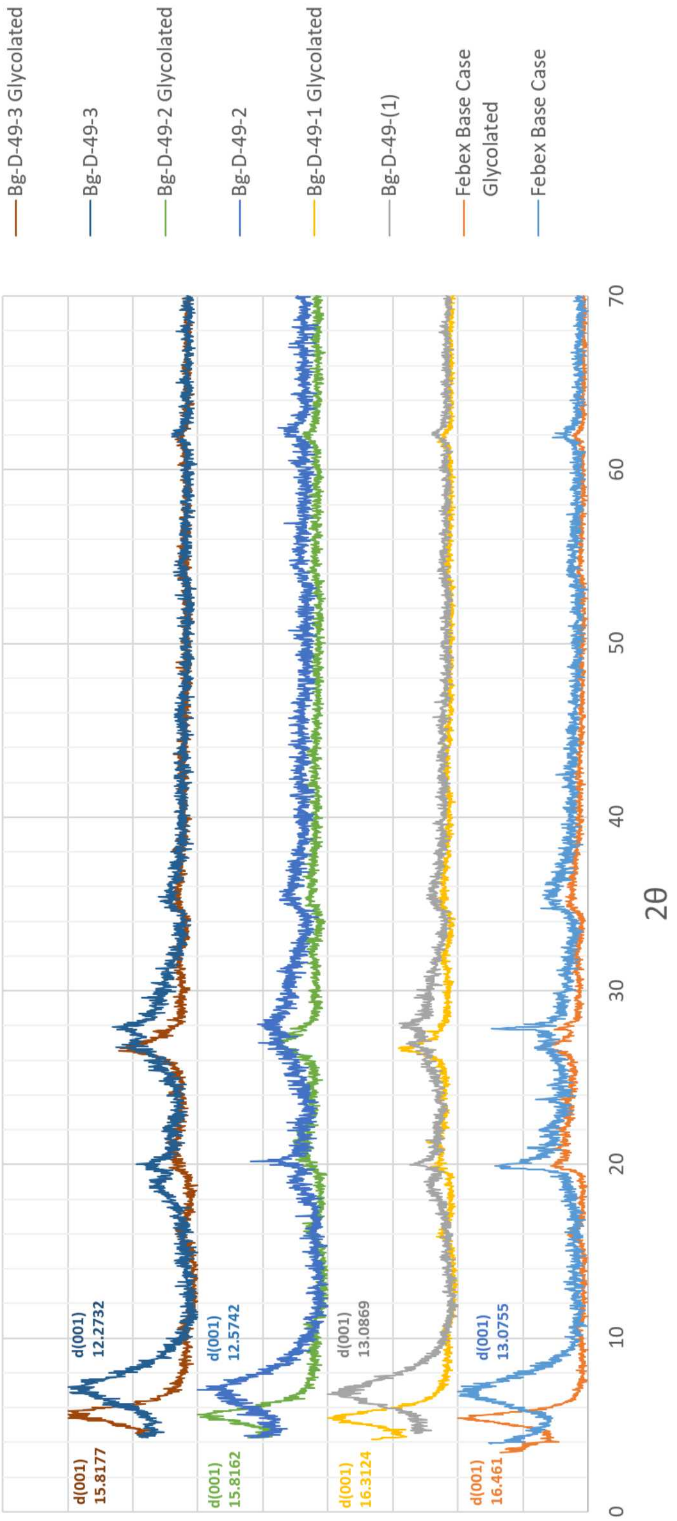

Figure A-13. XRD spectra (air-dried and glycolated) for various positions of BG-D-49 samples in the same blocks along with d-spacings (see schematic Fig. 3 for sample locations). XRD spectrum of FEBEX base case or reference material is shown at the bottom for comparison. These are the most distal bentonite samples from the heater surface.